ANALYSIS AND DESIGN OF FERROELECTRIC-RESONANT TRIGGER PAIR

CHARLES E. GREMER

ANALYSIS AND DESIGN

OF

FERROELECTRIC-RESONANT

TRIGGER PAIR

Charles E. Gremer

ANALYSIS AND DESIGN

OF

FERROELECTRIC-RESONANT

TRIGGER PAIR

by

Charles E. Gremer

Lieutenant, United States Navy

Submitted in partial fulfillment
of the requirements
for the degree of
MASTER OF SCIENCE
IN
ENGINEERING ELECTRONICS

United States Naval Postgraduate School
Monterey, California

1955

This work is accepted as fulfilling

the thesis requirements for the degree of

MASTER OF SCIENCE

IN

ENGINEERING ELECTRONICS

from the

United States Naval Postgraduate School

PREFACE

A modern high speed digital computer uses many vacuum tubes in bistable circuits. These circuits and hence the computer, are susceptible to the failures of the vacuum tubes. Although considerable progress has been made towards improving the reliability of vacuum tubes, they do not approach that of the later-developed "solid-state" devices. In addition to greater reliability offered by these devices, the small size and low power consumption is particularly enticing where large numbers of bistable circuits are needed. In particular, the development of the ferrites and titanates for high permeability and dielectric constants introduced non-linear elements in a component size that surpasses the highly lauded transistor. As with other new circuit elements much is left to be done, especially in improvement of the materials involved. However, the first step was taken by C. F. Spitzer /7/ in the analysis of the two-branch, bistable, series resonant circuit, using a non-linear inductance. The next move is the analysis of the non-linear capacitor circuit which this paper purports to do. The next obvious step would be the inclusion of both devices in a single circuit, and a short development of this appears in hopes of beginning the solution to this problem.

The analysis is to be done with the thought in mind of obtaining a set of design equations for a circuit which might be used as a bi-

stable network. Both the two-branch, series resonant circuit, which consists of series elements in a parallel network, and the two-mesh, parallel resonant circuit, which consists of parallel elements in a series network, are analyzed. Consideration of triggering schemes, although of great importance, occupies a small portion of this paper since it was not the primary purpose to design an actual circuit but rather obtain the criteria which might lead to a realizable circuit. The production of an actual operating circuit awaits the development of materials with lower losses and slightly greater non-linearities. The necessary changes and the progress being made on this phase of the elements are entirely beyond the scope of this paper.

The author wishes to express his deep gratitude to Charles A. Rosen and Charles F. Spitzer of the General Electric Laboratories for their extensive suggestions and guidance in the completion of this paper. Without the many "skull" sessions with these gentlemen, this paper probably would not have been written.

TABLE OF CONTENTS

LIST OF ILLUSTRATIONS

TABLE OF SYMBOLS AND ABBREVIATIONS
(Listed in the order of their use in the text)

$\ddot{x}$	second derivative with respect to time of a variable x.
g	gravitational constant
a_1, a_3	constants of the charge-voltage
$\overset{M}{>}$	must be greater than
$\overset{M}{=}$	must be equal to
E_i, e_i	peak; instantaneous value of i th voltage
Q_i, q_i	peak; instantaneous value of i th change
q_{ij}	the j th iteration of i th charge
A, B	charge amplitudes
ψ_i	designator for the i th solution curve
s	parameter which measures relative "detuning"
ω_0	initial resonant frequency
m	parameter which measures the degree of non-linearity of non-linear capacitor
α, β	rotation parameters relating A and B
D	parameter measuring ratio of non-linearity to detuning
$\rho\ \theta$	polar coordinates for plotting solution curves
P_i	i th solution point
I_s, i_s	source current
φ	loss angle
Δ	switching ratio

b_1, b_3	constants of the current flux relationship for the non-linear inductance
N	number of wire turns on non-linear inductor
F	parameter to reduce equation size (see equation IV-13a
G	parameter to reduce equation size (see equation IV-13b
n	parameter which measures the degree of non-linearity in a non-linear inductor
l	parameter to reduce equation size (see equation IV-16c

CHAPTER I

INTRODUCTION

The circuits to be analyzed in this paper are the two-branch, series resonant circuit shown in figure I-1a; and the two-mesh, parallel resonant circuit shown in figure I-1b. Both of these circuits utilize only one non-linear element. In chapter IV a brief development appears of the two-branch, series resonant circuit using two non-linear elements as shown in figure I-2.

Inasmuch as these circuits contain non-linear elements, methods other than linear network analysis must be employed. There are several approaches for analyzing such circuits based upon developments by Duffing, Poincaré , Kryloff and Bogoliuboff and others [1, 2, 3, 4, and 8]. The choice of one approach over another depends on the accuracy desired, the accuracy obtainable, and the exact problem confronting the analyst. The method of Dryloff and Bogoliuboff is certainly more general than that of Poincaré; and both are more accurate than that of Duffing. On the other hand, the method of Duffing is far easier than the others and yet yields the desired information to a sufficient degree of accuracy. All of these methods mentioned are analytical and suffer from one inherent disadvantage: they produce solutions for only the case under consideration without any thought as to the totality of solutions available. A qualitative method, known as the topological approach, gives an overall picture of the

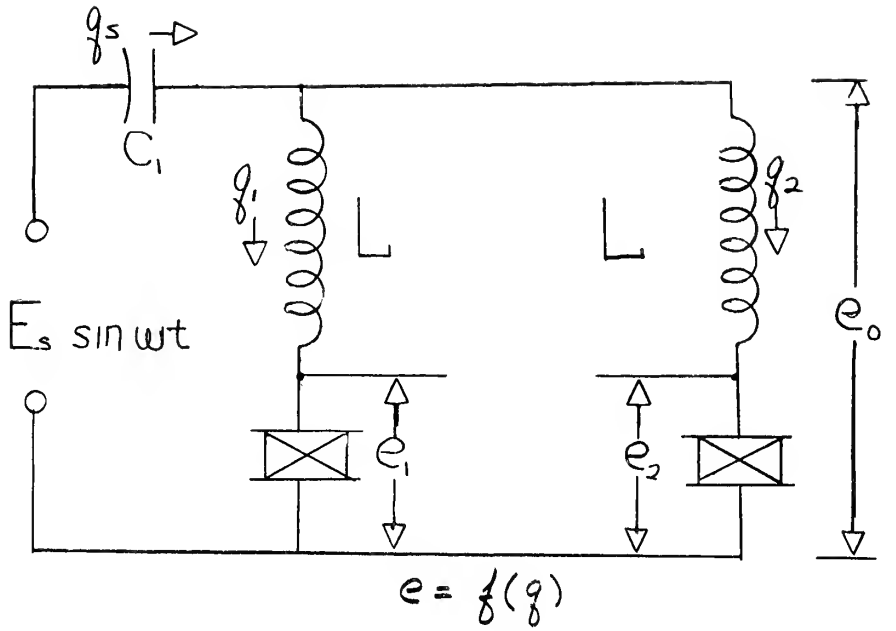

Figure I-1a Two Branch, Loss-Free Series Resonant Circuit

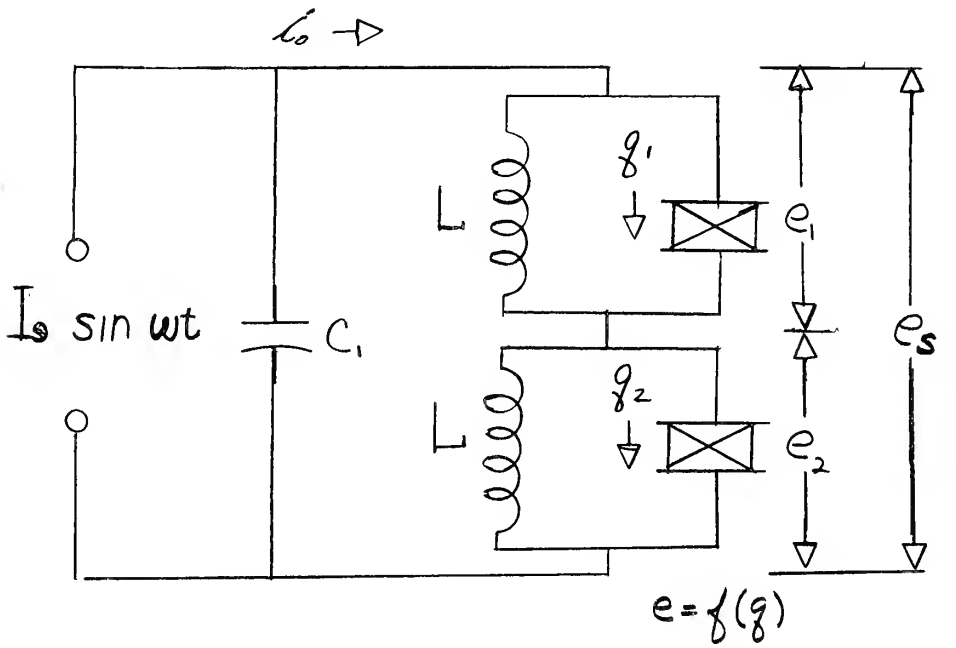

Figure I-1b Two-Mesh, Loss-Free Parallel Resonant Circuit

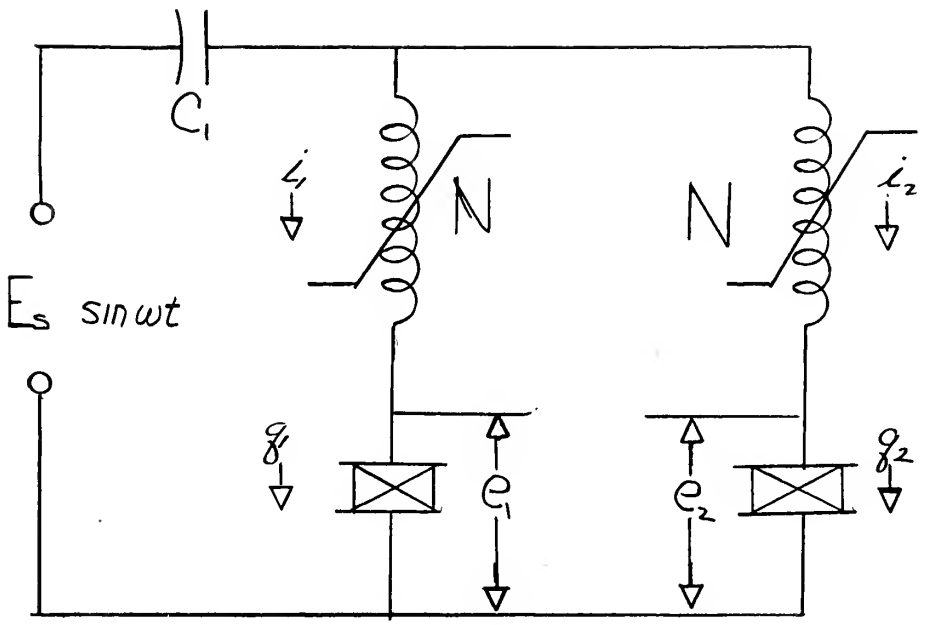

$$i_1 = f(\phi_1)$$
$$i_2 = f(\phi_2)$$
$$e_1 = g(q_1)$$
$$e_2 = g(q_2)$$
$$i = \frac{dq}{dt}$$
$$q = \int_0^t i\,dt$$

Figure I-2 A two-branch Loss-Free Series Resonant Circuit using Two Non-linearities

totality of solutions but yields no specific information on any particular case [1, 3, and 8].

The non-linear capacitors available at this writing had relatively large losses, were dependent on temperature, and had small non-linearities. Furthermore, there was no available test equipment for measuring the component parameters at the higher frequency of circuit operation. Finally, the determination of the component parameters was based on some rather sweeping assumptions and hence accuracy was sacrificed ab initio.

For these reasons, and due to its simplicity, a modified form of Duffing's method was chosen. In order to clearly understand the developments of chapters II through IV, a brief presentation of this method and the reasoning leading to it is given in what follows.

Consider the motion of a simple pendulum having no losses and not under the influence of an external force. The differential equation of this system, as shown in figure I-3 is

$$\ddot{x} + \frac{g}{\ell} \sin x = 0. \qquad \text{I-1}$$

The solution is begun by using the substitutions

$$\frac{dx}{dt} = v \; ; \quad \frac{d^2x}{dt^2} = \frac{dv}{dx}\frac{dx}{dt} = v\frac{dv}{dx}$$

Equation I-1 then becomes, after separating the variables:

$$v\,dv = -\frac{g}{\ell} \sin x \, dx. \qquad \text{I-2}$$

Integrating this expression gives:

$$v^2 = \frac{2g}{\ell}\cos x + h, \qquad \text{I-3}$$

where h is the energy constant of the system. From this equation a plot of v versus x is made as shown in figure I-4. From equation I-3 and the plots of figure I-4, the following observations can be made:

1) $h \leq 0$ or v^2 becomes negative, which defines an unrealistic case:

2) if $-\frac{2g}{\ell} < h < \frac{2g}{\ell}$, the curves are closed, encircle the points $v = 0$, $x = 2n\pi$, n being an integer, and hence the pendulum oscillates about the angle $x = 2n\pi$; and

3) if $h > \frac{2g}{\ell}$, v is never zero, and thus the pendulum continues to rotate about its pivot.

The heavy plot corresponds to the case $h = \frac{2g}{\ell}$, and it can be shown that this case cannot exist. However, this value of h divides the totality of solutions: those that are periodic and those that are aperiodic.

This procedure just outlined represents the crux of the topological approach. From it there has been determined, once and for all, the totality of solutions in the system, but nothing has been learned as to the values associated with any particular case.

It seems evident that if a driving force were included, then whether or not the solutions were periodic or aperiodic would depend on the amount of energy this force adds to the original system.

Obviously, if aperiodic solutions are allowed in the electrical

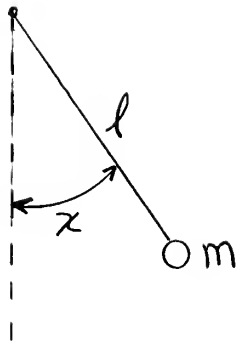

Figure I-3 Simple Pendulum

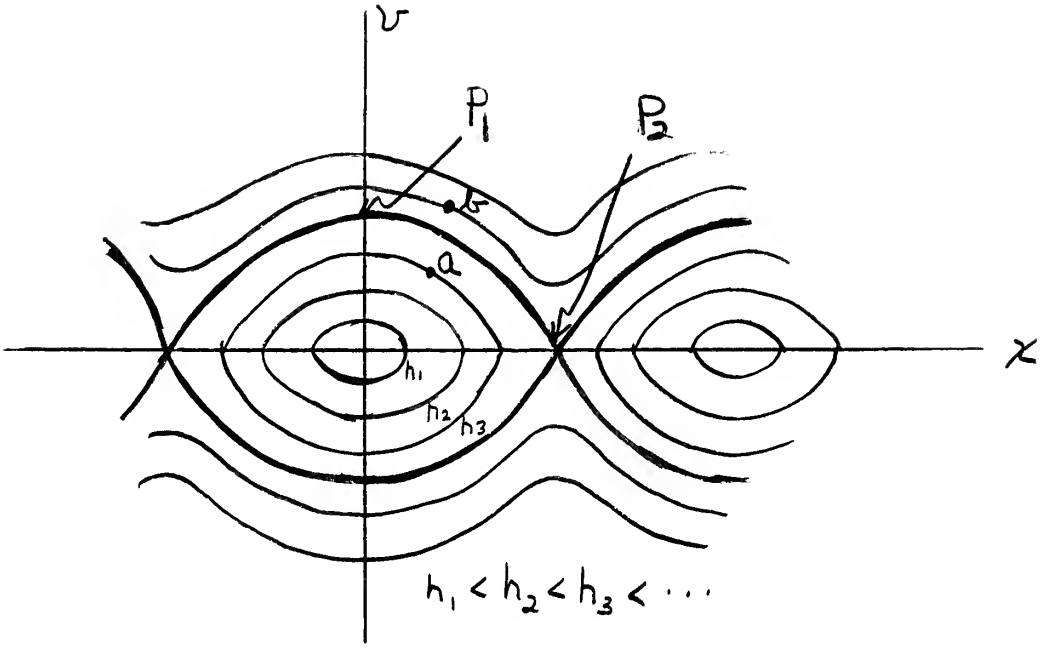

Figure I-4 Velocity versus displacement curves for simple pendulum.

circuit cases, then, at some time, the currents and/or charges will be of sufficient magnitude to destroy the circuit elements. Thus analysis can immediately refrain from these solutions and concentrate on those in which periodicity is mandatory.

In order to obtain these periodic solutions we now consider Duffing's method which was first applied to the equation bearing his name:

$$\ddot{x} + c\dot{x} + a_1 x + a_3 x^3 = F\cos\omega t. \qquad \text{I-4}$$

Note that the function of x appearing in this equation resembles the first two terms of the expansion of the sin x function. Hence, it might be expected that the solutions are much the same as those of equation I-1. Such is found to be the case within the region of periodic solutions [1 and 8].

First, assume no damping, i.e. c = 0, and write the equation in the following form:

$$\ddot{x} = -a_1 x - a_3 x^3 + F\cos\omega t. \qquad \text{I-5}$$

The iteration now starts with the first approximation (the approximation x = 0 being considered trivial), $x_0 = A\cos\omega t$, and inserts this into the right hand side of equation I-5. This obtains:

$$\ddot{x}_1 = -(a_1 A + \tfrac{3}{4} a_3 A^3 - F)\cos\omega t - \tfrac{1}{4} a_3 A^3 \cos 3\omega t. \qquad \text{I-6}$$

Integrating this expression twice, there results

$$x_1 = \frac{1}{\omega^2}(a_1 A + \tfrac{3}{4} a_3 A^3 - F)\cos\omega t + \frac{a_3}{36\omega^2} A^3 \cos 3\omega t, \qquad \text{I-7}$$

the constants of integration having vanished in order to preserve

periodicity.

At this point Duffing made a rather far reaching choice. In lieu of the usual procedure of prescribing ω and then determining the amplitude, A_1, of the fundamental, he prescribed $A_1 = A$ and thus obtained

$$\omega^2 = a_1 + \frac{3}{4} a_3 A^2 - \frac{F}{A} . \qquad \text{I-8}$$

It is noted that ω becomes a single-valued function of A but that A could be a triple-valued function of ω . It was for this reason that A was prescribed, and hence, ω determined.

The next step of the iteration procedure would be to substitute the solution

$$x_1 = A \cos \omega t + \frac{a_3 A^3}{36\omega^2} \cos 3\omega t$$

into the right hand side of equation I-5 and again integrate twice letting the constants of integration vanish. This, then, is Duffing's method. For rapid convergence a_3 and A should be small.

The modified procedure used in this paper removes the restrictions on a_3 and A, but implies that the driving force is small of order a_3 i.e. we set $F = a_3 F_0$.

This begins by adding $\omega^2 x$ to both sides of I-5 and obtaining:

$$\ddot{x} + \omega^2 x = (\omega^2 - a_1) x - a_3 x^3 + a_3 F_0 \cos \omega t. \qquad \text{I-9}$$

Again, iteration starts with the approximation $x_0 = A\cos\omega t$ and substitutes this into the right hand side of equation I-9.

This gives:

$$\ddot{x}_1 + \omega^2 x_1 = \left[(\omega^2 - a_1) A - \frac{3}{4} a_3 A^3 + a_3 F_0\right] \cos \omega t - \frac{1}{4} a_3 A^3 \cos 3\omega t. \qquad \text{I-10}$$

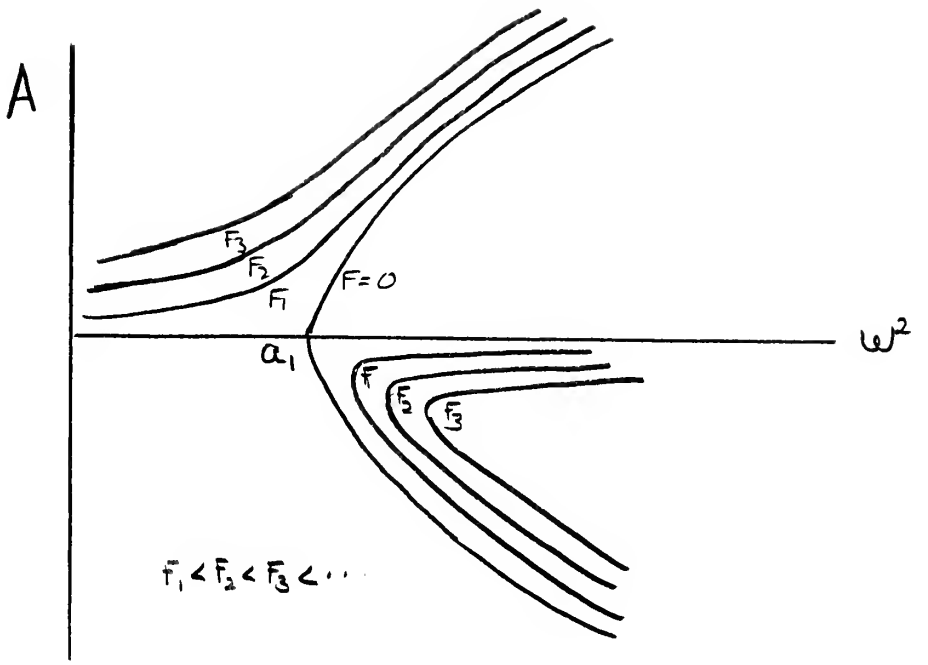

Figure I-5a A, Relationship for Duffing's Equation

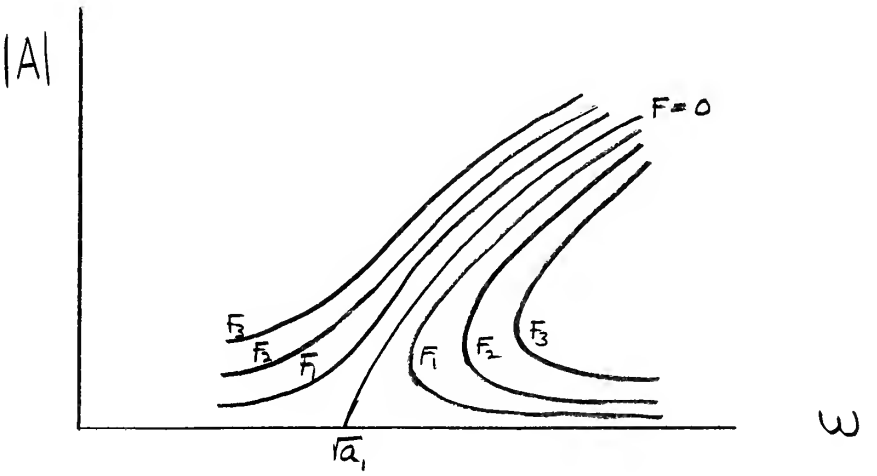

Figure I-5b A Response Curves for Duffing's Equation

Now to perform the next step in the iteration it is noted that the coefficient of $\cos\omega t \stackrel{M}{=} 0$ or else secular terms of the type $Bt\cos\omega t$ arise.

This procedure gives:

$$(\omega^2 - a_1)A - \frac{3}{4}a_3 A^3 + a_3 F_0 = 0$$

or

$$\omega^2 = a_1 + \frac{3}{4}a_3 A^2 + \frac{a_3 F_0}{A} \qquad \text{I-11}$$

which is precisely the same relation resulting before if $a_3 F_0$ is replaced by F. After setting the $\cos\omega t$ term to zero, there results:

$$\ddot{x}_1 + \omega^2 x_1 = -\frac{1}{4}a_3 A^3 \cos 3\omega t$$

which gives as its solution

$$x_1 = A_1 \cos\omega t + \frac{a_3}{32\omega^2} A^3 \cos 3\omega t. \qquad \text{I-12}$$

As in Duffing's method the choice is to make $A_1 = A$. The procedure is then to substitute I-12 into the right hand side of equation I-9 and repeat the steps above. The iteration is continued until the desired degree of accuracy is obtained.

It is instructive, and will be useful later, to plot equation I-8. Although ω^2 is the dependent variable in this case, it is plotted on the abcissa in order to show the resemblance of the response curves to the linear case. The plots in figure I-5 are for the lossless case, while those in figure I-6 are for the case where losses are considered [8]. It might be added parenthetically at this point that the plots in these figures bend to the right or left according to whether a_3 is greater or less than zero respecitvely. If a_3 is zero, the linear case results and the curves are upright.

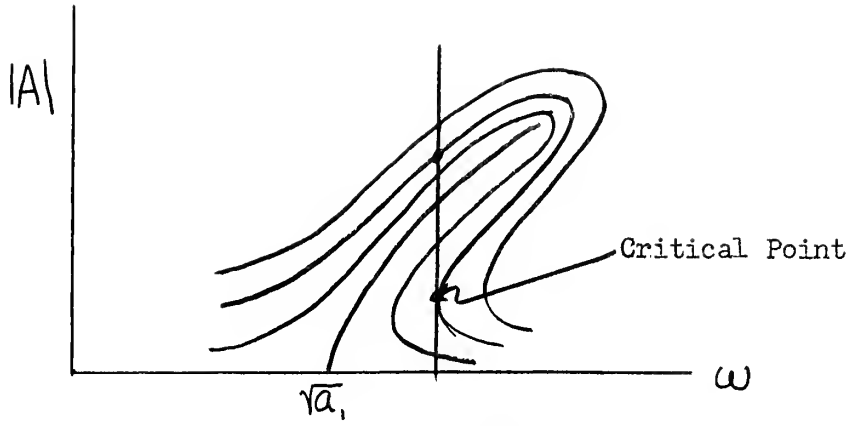

Figure I-6 A for Duffing's Equation Low-Loss Case

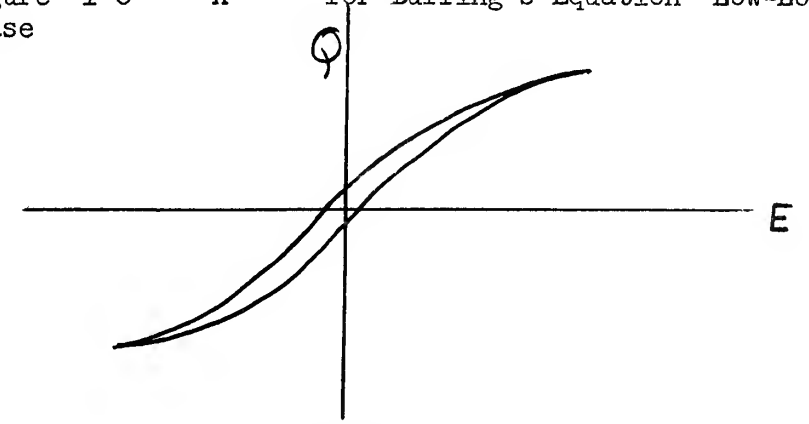

Figure I-7 Q-E Relationship for A Non-Linear Capacitor

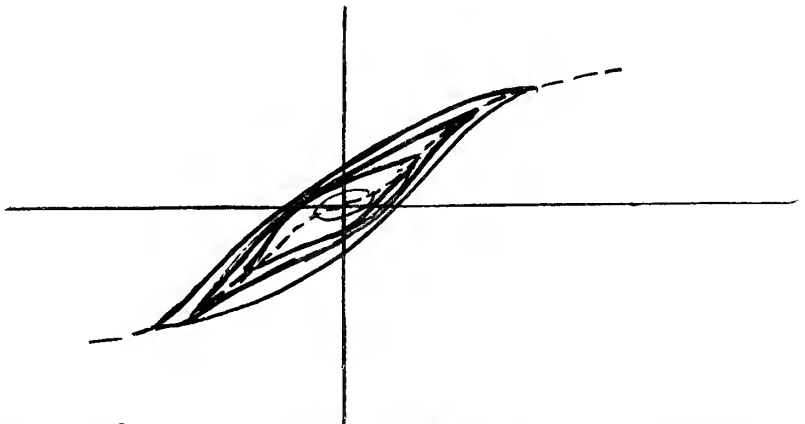

Figure I-8 Nest of Q-E Curves for Varying Field Amplitudes

If a single series circuit were to be driven with a constant frequency source whose amplitude could be made to vary, then operation would take place along a vertical line such as that shown in figure I-5a. It should be noted that as the amplitude of the driving force is slowly increased a point is reached where there are two possible values of the response, A. Since A represents charge in the electrical case, and current is the time rate of change of charge, when this critical force is reached, the current is said to jump. If, instead of a single series circuit, two such circuits are placed in parallel as in figure I-1a, and a constant current source used, it would seem plausible that when the critical force level is reached, one branch current would "jump" up while the other branch current would "jump" down. Such an event does occur.

The question now arises as to what form f(q), shown in figure I-1, shall take. If a charge versus voltage plot is taken on one of these non-linear capacitors, a curve such as that shown in figure I-7 results. This particular curve is for one value of driving voltage. In figure I-8 a set of such loops is shown for various driving amplitudes. The heavy line connects the loop tips. Obviously, no simple relation defines the Q-E curves of either figure I-7 or I-8.

Since the real interest is in the value of charge which can cause bistability, it would seem evident that the large signal loops are of more importance. This is due to the fact that the charges must be large enough to cause an excursion into the non-linear region at the time of "jumping" into bistability.

If a single-valued function is desired, it is assumed that the Q-E relationship follows the mid-points rather than the upper or lower portions of the loops. This tends to average the characteristics and has the advantage that voltage is zero when the charge is zero.

The assumptions made this far are the primary limitation on the accuracy of any solution. It would seem rather irrational to choose an involved functional relationship however accurate it may be. Thus the defining relation is chosen as:

$$e = a_1 q + a_3 q^3, \qquad \text{I-13}$$

an odd function which is required for the midpoint loci.

The necessary information has now been obtained in order to commence the analysis of the bistability problem.

CHAPTER II

TWO-BRANCH, SERIES RESONANT CIRCUIT

It is the plan of this chapter to investigate the two-branch, series resonant circuit. Investigation first concerns itself with the loss-free circuit in order to determine the basic relationships for bistability. After these conditions have been studied, emphasis will shift to the low-loss circuit, in an effort to determine the effect of resistance on the bistability relationships.

SECTION I: THE LOSS-FREE CIRCUIT

The equations of the circuit of figure I-1a can be written as follows:

$$e_s = L\frac{d^2q_1}{dt^2} + e_1 + \frac{q_1+q_2}{C} \qquad \text{II-1a}$$

$$e_s = L\frac{d^2q_2}{dt^2} + e_2 + \frac{q_1+q_2}{C}. \qquad \text{II-1b}$$

Subtracting equation II-1b from II-1a, there is obtained one of the basic equations for the circuit:

$$L\frac{d^2(q_1-q_2)}{dt^2} + e_1 - e_2 = 0. \qquad \text{II-2}$$

The other basic equation for the circuit is:

$$q_s = q_1 + q_2 \,. \qquad \text{II-3}$$

As in chapter I the defining relations for e_1 and e_2 are chosen as

$$e_1 = a_1 q_1 + a_3 q_1^3 \qquad \text{II-4a}$$

$$e_2 = a_1 q_2 + a_3 q_2^3 \,. \qquad \text{II-4b}$$

Since it was decided that the circuit should have a constant current source, the impedance seen by the generator voltage, e_s, must be that offered by C_1, otherwise the varying impedance offered by the two non-linear branches would vitiate the constant current hypothesis. Thus i_s leads e_s and hence, since it was tacitly assumed that there were no losses, the first iteration begins with:

$$q_{10} = A \sin \omega t \qquad \text{II-5a}$$

$$q_{20} = B \sin \omega t \,, \qquad \text{II-5b}$$

where the second subscript denotes the iteration by which the value was obtained.

Equation II-2 is rewritten as follows:

$$(\ddot{q}_1 - \ddot{q}_2) + \omega^2 (q_1 - q_2) = \omega^2 (q_1 - q_2) - \frac{1}{L}(e_1 - e_2) \,. \qquad \text{II-6}$$

The next step is to substitute equations II-5a and II-5b into the right hand side of equation II-6. This results in (see appendix III for expansions of powers of trigonometric functions):

$$(\ddot{q}_1-\ddot{q}_2)_1+\omega^2(q_1-q_2)_1=\left[(\omega^2-\frac{a_1}{L})(A-B)-\frac{3a_3}{4L}(A^3-B^3)\right]\sin\omega t$$
$$+\frac{a_3}{4L}(A^3-B^3)\sin 3\omega t. \qquad \text{II-7}$$

The conditions for periodicity require that:

$$(\omega^2-\frac{a_1}{L})(A-B)-\frac{3a_3}{4L}(A^3-B^3)=0. \qquad \text{II-8}$$

Disregarding the trivial case of A = B and using equations II-3 and II-5 there results two equations relating A and B:

$$\Psi_1\equiv 0=-Q_S+A+B \qquad \text{II-9}$$

$$\Psi_2\equiv 0=-S+m(A^2+AB+B^2); \qquad \text{II-10}$$

where

$$S=\frac{\omega^2}{\omega_0^2}-1, \qquad \text{II-11}$$

$$\omega_0^2=\frac{a_1}{L}, \qquad \text{II-12}$$

$$m=\frac{3}{4}\frac{a_3}{a_1}. \qquad \text{II-13}$$

Ψ_1 is a straight line whereas Ψ_2 is an ellipse. Using the rotation matrix

$$\begin{bmatrix}A\\B\end{bmatrix}=\begin{bmatrix}\frac{1}{\sqrt{2}} & -\frac{1}{\sqrt{2}}\\ \frac{1}{\sqrt{2}} & \frac{1}{\sqrt{2}}\end{bmatrix}\begin{bmatrix}\alpha\\\beta\end{bmatrix} \qquad \text{II-14}$$

equation II-10 becomes:

$$\Psi_2\equiv 0=-\frac{S}{m}+3\alpha^2+\beta^2. \qquad \text{II-15}$$

The half axes are

$$a_\alpha = \sqrt{\frac{2S}{3m}}, \quad \text{and} \qquad \text{II-16}$$

$$a_\beta = \sqrt{\frac{2S}{m}}. \qquad \text{II-17}$$

For the two-branch series resonant circuit the second iteration must be performed in order to obtain bistability conditions. The only information obtainable from the above relations, is that in order to have real solutions of ψ_2, $S \overset{M}{>} 0$ and hence $\omega \overset{M}{>} \omega_0$, where $\overset{M}{>}$ means: "must be greater than". This condition can be deduced intuitively as follows. For bistability $A \neq B$ and hence one of the two identically designed branches must offer less opposition to charge movement than the other, due to the non-linearity of its branch capacitance. This requires one branch to be "tuned" nearer to ω than the other. Now for a capacitor defined by an equation such as II-4, it is found that the effective capacitance presented to the fundamental voltage decreases as the amplitude of the impressed, fundamental voltage increases. Hence as the amplitude of voltage increases, the resonant frequency of the branch must increase. Hence the circuits must originally be tuned below the source frequency i.e. $\omega > \omega_0$. Thus, what was intuitively believed has been proven by the inequality, $S \overset{M}{>} 0$.

Solving equation II-7, after the condition of periodicity has been invoked, there is thus obtained

$$(q_1 - q_2)_1 = (A_1 - B_1)\sin \omega t - \frac{a_3}{32\omega^2 L}(A^3 - B^3)\sin 3\omega t. \qquad \text{II-18}$$

The choice as explained in chapter I, is to make $A_1=A$ and $B_1=B$. Equating the portions of II-7 identifiable with q_1 and q_2 respectively, there results

$$q_{11} = A \sin \omega t - DA^3 \sin 3\omega t \qquad \text{II-19a}$$

$$q_{21} = B \sin \omega t - DB^3 \sin 3\omega t \qquad \text{II-19b}$$

where

$$D = \frac{a_3}{32\omega^2 L} = \frac{m}{24(s+1)}. \qquad \text{II-20}$$

Substituting these relationships into the right hand side of equation II-6 there results (see Appendix II for details of the mathematical development):

$$(\ddot{q}_1 - \ddot{q}_2)_2 + \omega^2(q_1 - q_2)_2 =$$

$$\left[(\omega^2 - \frac{a_1}{L})(A-B) - \frac{3a_3}{4L}(A^3 - B^3)\right.$$

$$\left. - D\frac{3a_3}{4L}(A^5 - B^5) - D^2\frac{3a_3}{2L}(A^7 - B^7)\right] \sin \omega t$$

$$+ \left[\frac{a_3}{4L}(A^3 - B^3) + \frac{3a_3}{2L}D(A^5 - B^5) + \frac{3a_3}{4L}D^3(A^9 - B^9)\right] \sin 3\omega t$$

$$- \left[\frac{3a_3}{4L}D(A^5 - B^5) + \frac{3a_3}{4L}D^2(A^7 - B^7)\right] \sin 5\omega t$$

$$+ \left[\frac{3a_3}{4L}D^2(A^7 - B^7)\right] \sin 7\omega t$$

$$+ \frac{a_3}{4L}D^3(A^9 - B^9) \sin 9\omega t. \qquad \text{II-21}$$

Invoking the condition of periodicity and disregarding the trivial solution, A = B, there results:

$$\psi_3 \equiv 0 = -S + m(A^2 + AB + B^2) + mD(A^4 + A^3B + A^2B^2 + AB^3 + B^4)$$

$$+ 2mD^2(A^6 + A^5B + A^2B^4 + A^3B^3 + A^2B^4 + AB^5 + B^6). \qquad \text{II-22}$$

Using the rotation matrix of equation II-14, equation II-22 becomes

$$\psi_3 \equiv 0 = -\frac{S}{m} + \frac{1}{2}(3\alpha^2 + \beta^2) + \frac{D}{4}(5\alpha^4 + 10\alpha^2\beta^2 + \beta^4)$$

$$+ \frac{D^2}{4}(7\alpha^6 + 35\alpha^4\beta^2 + 21\alpha^2\beta^4 + \beta^6). \qquad \text{II-23}$$

This form is still not too instructive. However, another transformation reduces the form to where the desired results can be obtained. Letting $\alpha = \rho\cos\theta$ and $\beta = \rho\sin\theta$, II-23 becomes:

$$\psi_3 \equiv 0 = -\frac{S}{m} + \frac{1}{2}f(\theta)\rho^2 + \frac{D}{4}g(\theta)\rho^4 + \frac{D^2}{4}h(\theta)\rho^6 \qquad \text{II-24}$$

where

$$f(\theta) = 2 + \cos 2\theta, \qquad \text{II-25a}$$

$$g(\theta) = 3.5 + 2\cos 2\theta - 0.5\cos 4\theta \qquad \text{II-25b}$$

and

$$h(\theta) = 15 + \cos 2\theta[4 - 18\cos 2\theta - \cos^2 2\theta] + 7\cos 4\theta. \qquad \text{II-25c}$$

For any value of θ, ψ_3 has only two finite, real roots (positive and negative values of the same magnitude) and hence represents a single closed loop. ψ_1, ψ_2 and ψ_3 are shown in figure II-1. The developments of these curves and the proof of the single root magnitudes are shown in Appendix II.

From figure II-1, the mode of operation may be explained. For

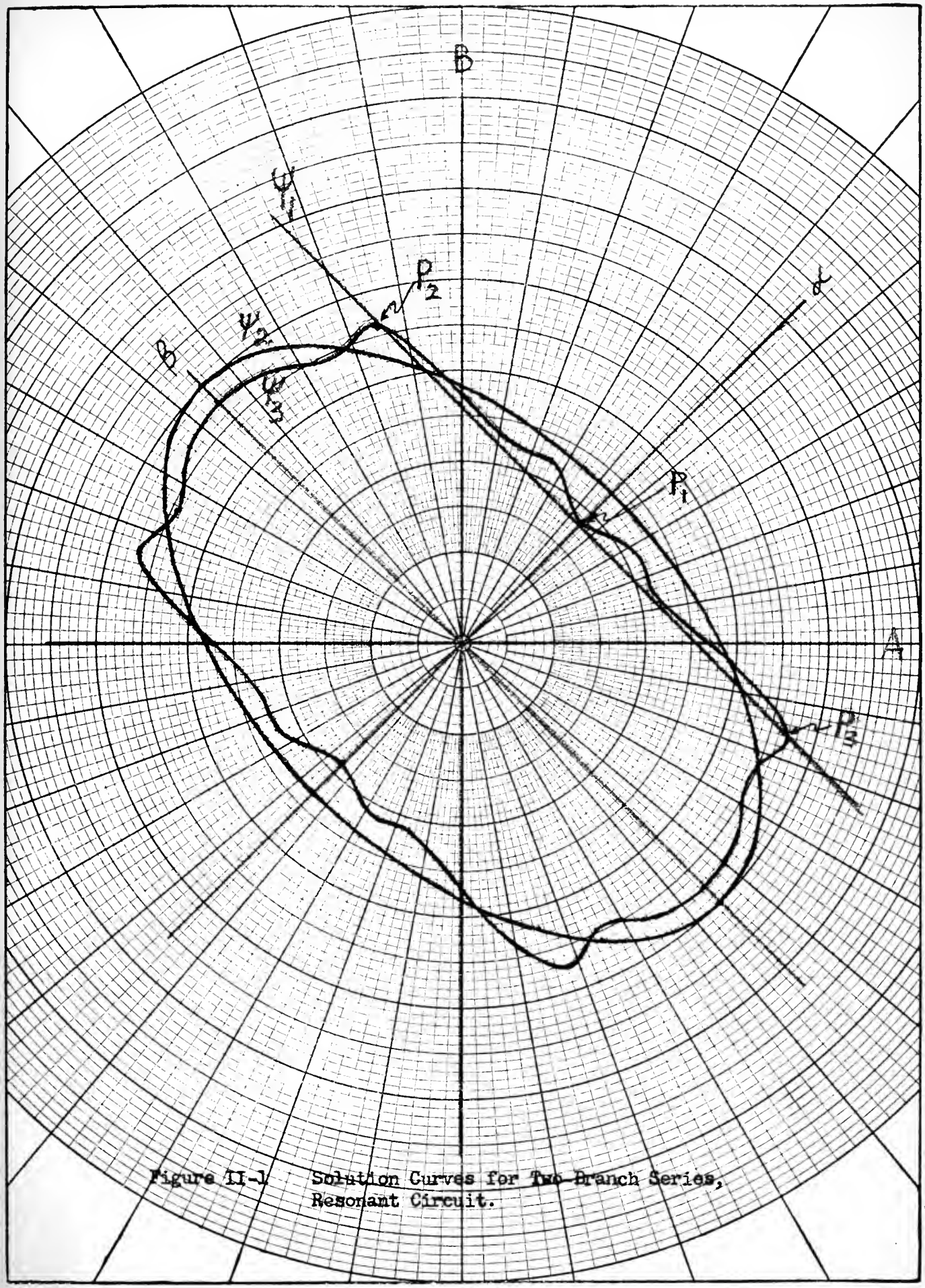

Figure II-1 Solution Curves for Two-Branch Series, Resonant Circuit.

small values of E_s, and hence Q_s, the two series branches behave as linear networks and thus A = B. As E_s is increased, ψ_1 moves out from the origin parallel to the β axis. The operating point remains on the intersection of ψ_1 and the line, A = B. In Appendix II it is shown that for θ = 0 degrees, the slope of the tangent of ψ_3 is parallel to the β axis. Hence ψ_1 will be tangent to ψ_3 at the operating point P_1. When ψ_1 becomes tangent to ψ_3, there are now, two other operating points available, P_2 and P_3. Although no mathematical proof is given here, it can be deduced from the work of Stoker [8] that the area around P_1 is unstable. Operation, therefore, "jumps" to either P_2 or P_3. The reasons leading to this deduction of P_1 being unstable are given in chapter III for the first iteration of the two-mesh parallel circuit. The reason for postponing this discussion until then is apparent from the discussion itself.

A circuit in which the controlled switching of the operating point from P_2 to P_3, or vica versa, is obtainable constitutes a trigger pair.

The reader might now infer that the first iteration will not predict bistability for the two-branch series resonant circuit. However, in chapter III it will be shown that this is an unwarranted conclusion; the same value of E_s which will cause bistability will be predicted by two different approaches.

For operating point P_1 in figure II-1, the following values, developed in appendix II, are obtained (θ = 0°):

$$\rho_{\theta=0^\circ} = \frac{.756}{\sqrt{D}}\left[1.68\sinh u - 0.417\right]^{1/2} \qquad \text{II-26}$$

$$u = \frac{1}{3}\sinh^{-1}\frac{.916S + .805}{S+1} \qquad \text{II-27}$$

$$Q_S = A + B = 2A = \sqrt{2}\,\rho_{\theta=0^\circ} \qquad \text{II-28}$$

$$I_S = \omega Q_S \qquad \text{II-29}$$

Obviously, if ψ_1 moves out from the origin so far that is fails to intersect ψ_3, bistability fails to exist and both branches revert to equal currents. Form figure II-1 this appears to occur when is tangent to ψ_3 at about $\theta = 20^\circ$. For this condition, the value of I_S becomes

$$I_S = \omega Q_S = \omega \rho_{\theta=20^\circ}\left[\cos 20^\circ + \sin 20^\circ\right]$$

$$= \sqrt{2}\,\omega\rho_{\theta=20^\circ}\sin 65^\circ. \qquad \text{II-30}$$

Greater accuracy can be obtained by finding the value at which $\frac{d\alpha}{d\beta}$ vanishes, but this hardly seems like a reasonable procedure in view of the original assumptions.

It should be added at this point that after bistability occurs, there is no assurance that increasing E_S will increase I_S. This is due to the phase relationships possible between A and B. If the two operating points are located in the first quadrant of figure II-1, then A and B are in phase. If the two operating points are located in the second or fourth quadrants, then A and B are 180 degrees out of phase.

SECTION 2: THE LOW-LOSS CIRCUIT

Attention is now given to the case where the two branches contain losses as shown in figure II-2. Equation II-6 is rewritten to include the effect of resistance as follows:

$$(\ddot{q}_1-\ddot{q}_2)+\omega^2(q_1-q_2)=\omega^2(q_1-q_2)-\frac{R}{L}(\dot{q}_1-\dot{q}_2)-\frac{1}{L}(e_1-e_2). \qquad \text{II-31}$$

Assuming that R is small compared to X_{C_1}, then I_s will still be primarily determined by the impedance of C_1. For the remainder of the discussion in this chapter, it will be assumed that $A \gg B$. Hence, I_1 is very nearly in phase with I_s. Since I_s will lead E_s by 90 degrees, the first iteration begins with the approximations:

$$q_{10} = A \sin \omega t \qquad \text{II-32a}$$

$$q_{20} = B \sin(\omega t - \varphi) \qquad \text{II-32b}$$

Substituting these values into the right hand side of equation II-31, there is obtained thereby:

$$\begin{aligned}(\ddot{q}_1-\ddot{q}_2)+\omega^2(q_1-q_2) = {} & \left[(\omega^2-\tfrac{a_1}{L})A-\tfrac{3a_3}{4L}A^3\right]\sin\omega t \\ & -\left[(\omega^2-\tfrac{a_1}{L})B-\tfrac{3a_3}{4L}B^3\right]\sin(\omega t-\varphi) \\ & -\tfrac{R\omega}{L}A\cos\omega t+\tfrac{R\omega}{L}B\cos(\omega t-\varphi) \\ & +\tfrac{a_3}{4L}A_3\sin\omega t-\tfrac{a_3}{4L}B^3\sin 3(\omega t-\varphi). \qquad \text{II-33}\end{aligned}$$

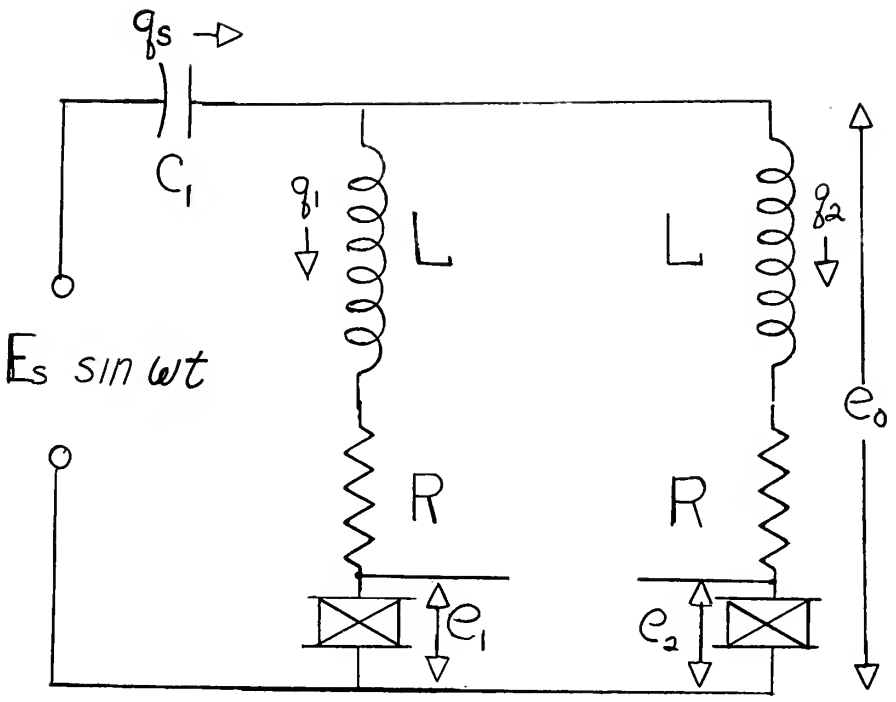

Figure II-2

Two-Branch Low-Loss Series Resonant Circuit

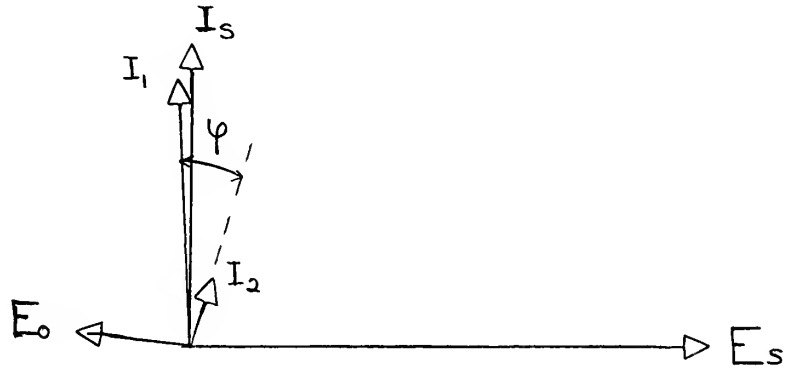

Figure II-3

Phase Relationships for Two-Branch, Low-Loss Series Resonant Circuit.

In order to preserve periodicity all of the fundamental component terms of ω must vanish identically. Hence there results:

$$\left[-sB + mB^3\right]\sin(\omega t - \varphi) + \frac{\omega R}{a_1} B \cos(\omega t - \varphi)$$

$$= \left[-sA + mA^3\right]\sin\omega t + \frac{\omega R}{a_1} A \cos\omega t, \qquad \text{II-34}$$

Expanding the terms involving $(\omega t - \varphi)$ and equating the coefficients of sin wt and cos wt respectively, there results:

$$\left[-sB + mB^3\right]\cos\varphi + \frac{\omega R}{a_1} B \sin\varphi = \left[-sA + mA^3\right], \qquad \text{II-35a}$$

$$\frac{\omega R}{a_1} B \cos\varphi - \left[-sB + mB^3\right]\sin\varphi = \frac{\omega R}{a_1} A \qquad \text{II-35b}$$

The phase diagram appears in figure II-3. Since R was presumed small, φ is very nearly zero degrees and hence cos $\varphi \approx 1$. Using this fact and dividing equation II-35a by II-35b, there results:

$$\frac{\frac{\omega R}{a_1} B \sin\varphi}{-\left[-sB + mB^3\right]\sin\varphi} = \frac{\left[-sA + mA^3\right] - \left[-sB + mB^3\right]}{\frac{\omega R}{a_1} A - \frac{\omega R}{a_1} B}$$

or

$$-s + m(A^2 + AB + B^2) = -\frac{\omega^2 R^2}{a_1^2} \cdot \frac{1}{s - mB^2} \qquad \text{II-36}$$

If R is allowed to vanish, the first iteration, loss-free case is immediately derivable from the above. Experimentally mB^2 is of the order 8×10^{-3} whereas s is unity or greater, so that the assumption, $s \gg mB^2$ is not too unreasonable. If it is allowed that $s \gg mB^2$ then II-36 reduces to

$$\psi_2' = 0 = A^2 + AB + B^2 - \frac{S}{m} + \frac{\omega^2 R^2}{a_1 S m} . \qquad \text{II-37}$$

Now ψ_2' will not be a real illipse, and hence bistability cannot result, unless

$$R < \frac{a_1 S}{\omega} , \qquad \text{II-38}$$

which places an upper limit on the losses.

For $B \neq 0$ II-37 gives

$$A = \pm \sqrt{\frac{S}{m} - \frac{\omega^2 R^2}{a_1^2 S m}} . \qquad \text{II-39}$$

If R is allowed to vanish, the first iteration, loss-free case is obtained, as can be seen from equation II-10.

From figure II-2, it can be seen that:

$$e_0 = L \ddot{q}_1 + R \dot{q}_1 + e_1 \qquad \text{II-40}$$

or

$$e_0 = a_1 \left\{ [-SA + mA^3] \sin \omega t + \frac{\omega R}{a_1} A \cos \omega t \right\} . \qquad \text{II-41}$$

The magnitude of E_0 can be found by first finding its square as:

$$E_0^2 = a_1^2 \left\{ [-SA + mA^3]^2 + \frac{\omega^2 R^2}{a_1^2} A^2 \right\} . \qquad \text{II-42}$$

Substituting the value of A from II-39, and upon simplification, there results:

$$E_0 = \omega R \sqrt{\left(\frac{S}{m} - \frac{\omega^2 R^2}{a_1^2 S m} \right) \left(1 + \frac{\omega^2 R^2}{a_1^2 S^2} \right)} . \qquad \text{II-43}$$

Since $B \approx 0$,

$$Z_2 = \sqrt{R^2 + \left(\omega L - \frac{a_1}{\omega}\right)^2}$$

$$= \frac{a_1}{\omega}\sqrt{\left(\frac{R\omega}{a_1}\right)^2 + S^2} \qquad \text{II-44}$$

and, since

$$I_2 = \omega B = \frac{E_0}{Z_2},$$

$$B = \frac{\omega R}{a_1 S}\sqrt{\left(\frac{S}{m} - \frac{\omega^2 R^2}{a_1^2 S m}\right)}. \qquad \text{II-45}$$

The ratio of A to B (i.e. the ratio of the larger to the smaller charge magnitudes) is defined as the switching ratio, Δ, and can be obtained from equations II-39 and II-45:

$$\Delta = \frac{a_1 S}{\omega R}. \qquad \text{II-46}$$

Now from equations II-4a and II-4b, remembering that $B \approx 0$, there results:

$$E_1 = a_1 A + a_3 A^3, \qquad \text{II-47a}$$

$$E_2 = a_1 B. \qquad \text{II-47b}$$

Since the usefulness of this circuit is predicated upon a sufficiently large difference between the two branch output voltages, it may be desirable to solve for this voltage difference: Hence, by sub-

traction, and by using equations II-39 and II-45 there results:

$$E_1 - E_2 = \left[a_1(1+s) - \frac{\omega R}{s}\left(\frac{\omega R}{a_1} - 1\right)\right]\sqrt{\frac{s}{m} - \frac{\omega^2 R^2}{a_1^2 s m}}, \qquad \text{II-48}$$

which for the loss-free case gives

$$E_1 - E_2 = a_1(1+s)\sqrt{\frac{s}{m}} \; . \qquad \text{II-49}$$

Thus it can be seen that although the switching ratio, Δ, is independent of the degree of non-linearity, m, that the voltage difference is inversely proportional to its square root. It should be noted, however, that Δ is not the ratio of E_1 to E_2, for the circuit under consideration. This value, still independent of m, is given by:

$$\frac{E_1}{E_2} = \frac{a_1 s}{\omega R}\left[1 + s - \frac{\omega^2 R^2}{a_1^2 s}\right]$$

$$= \Delta\left[1 + s - \frac{s}{\Delta^2}\right]. \qquad \text{II-50}$$

The smaller the value of m is, the larger the potential difference between the non-linear capacitors is for a given Δ. This follows from equation II-49 and the fact that Δ is related to the parameter, s, by equation II-46. This potential difference, however, is obtainable only by making A larger than B. But since the switching ratio, Δ, has been prescribed, both A and B increase, with B remaining in the linear region and A in the non-linear region of the Q-E relationship.

However, although Δ is independent of m, it must be remembered that too small a non-linearity results in currents of such magnitude

that they may destroy the components before bistability is reached.

All of the above relations were derived from the first iteration of the circuit with small losses. The second iteration is now commenced in order to find what modifications, if any, need to be made to the first iteration relations.

After the periodicity conditions have been invoked, equation II-33 becomes

$$(\ddot{q}_1 - \ddot{q}_2) + \omega^2(q_1 - q_2) = \frac{a_3}{4L} A^3 \sin 3\omega t$$

$$- \frac{a_3}{4L} B^3 \sin 3(\omega t - \varphi), \qquad \text{II-51}$$

whose solution is

$$(q_1 - q_2)_1 = (A_1 - B_1)\sin \omega t - DA^3 \sin 3\omega t$$

$$+ DB^3 \sin 3(\omega t - \varphi). \qquad \text{II-52}$$

Again choosing $A_1 = A$ and $B_1 = B$ there results, for the second approximations:

$$q_{11} = A \sin \omega t - DA^3 \sin 3\omega t \qquad \text{II-53a}$$

$$q_{21} = B \sin \omega t - DB^3 \sin 3(\omega t - \varphi). \qquad \text{II-53b}$$

Substituting these expressions into the right hand side of II-31, gives:

$$(\ddot{q}_1 - \ddot{q}_2)_2 + \omega^2(q_1 - q_2) =$$

$$\left[\omega^2 - \frac{a_1}{L}\right)(A - B) - \frac{3a_3}{4L}(A^3 - B^3) - \frac{3}{2} D^2 \frac{a_3}{L}(A^7 - B^7)\Big] \sin \omega t$$

$$\frac{3a_3}{4L} DA^5 \sin \omega t + \frac{3a_3}{4L} DB^5 \sin(\omega t - 3\varphi)$$

$$- \frac{\omega R}{L}(A-B)\cos\omega t$$

$$+ \cdots\cdots\cdots\cdots, \qquad \text{II-54}$$

where the dots refer to terms involving $3\omega t$, $5\omega t$, $7\omega t$ and $9\omega t$.

The conditions for periodicity become:

$$-\frac{\omega R}{L}(A-B) + \frac{3a_3}{4L} D B^5 \sin 3\varphi = 0 \qquad \text{II-55}$$

$$\left[\left(\omega^2 - \frac{a_1}{L}\right)(A-B) - \frac{3a_3}{4L}(A^3-B^3) - \frac{3a_3}{4L} D(A^5 - B^5\cos 3\varphi)\right.$$
$$\left. - \frac{3a_3}{2L} D^2(A^7-B^7)\right] = 0. \qquad \text{II-56}$$

From II-55, the phase relationship is determined as

$$\sin 3\varphi = \frac{4\omega R}{3a_3}\,\frac{(A-B)}{B^5}. \qquad \text{II-57}$$

Thus, since $\sin 3\varphi \overset{M}{\leq} 1$,

$$R \leq \frac{3a_3}{4\omega}\,\frac{B^5}{(A-B}. \qquad \text{II-58}$$

Solving for A-B results in:

$$A-B \leq \frac{3a_3}{4\omega R} B^5$$

$$\Delta - 1 \leq \frac{3a_3}{4\omega R} B^4$$

$$\Delta \leq \frac{a_1 S}{\omega R}\,\frac{m B^4}{S} + 1. \qquad \text{II-59}$$

Assuming that equation II-46 does in fact give a reasonable approximation for Δ, there results, upon substituting into II-59

$$\Delta \leq \frac{S}{S - m B^4}. \qquad \text{II-60}$$

Here again since bistability implies a value of Δ greater than unity, a small value of m may necessitate a value of B so large that the components themselves might be destroyed.

Substituting equation II-57 in equating II-56 and by using the first two terms of the expansion of $\cos 3\varphi$, there results, assuming φ to be small:

$$S(A-B) - m(A^3-B^3) - m\Delta\left(A^5-B^5+\frac{2\omega R}{3a_3}\sin 3\varphi(A-B)\right)$$

$$- 2m\Delta^2(A^7-B^7) = 0. \qquad \text{II-61}$$

Collecting terms, excluding the trivial solution, A=B; applying the rotating matrix, II-14; and using the polar coordinate form, there results for $\theta = 0^\circ$:

$$\rho_{\theta=0^\circ} = \frac{.756}{\sqrt{D}}\left[1.68\sinh 3\nu - .417\right]^{1/2} \qquad \text{II-62}$$

$$\nu = \tfrac{1}{3}\sinh^{-1}\left[\frac{.9165+.805}{S+1} - \frac{2.03\omega^2RD^2}{3a_3}\sin 3\varphi\right] \qquad \text{II-63}$$

Except for large values of R and φ, ν is approximately equal to μ as given by equation II-27.

Briefly summarizing these results:

1) in order to have bistability

$$I_s = \frac{\sqrt{2}\omega}{\sqrt{D}}(.756)\left[1.68\sinh 3\mu - .417\right]^{1/2} \qquad \text{II-26}$$

where $$\mu = \tfrac{1}{3}\sinh^{-1}\frac{.9165+.805}{S+1}\,; \qquad \text{II-27}$$

2) the switching ratio is given by

$$\Delta = \frac{a_1 S}{\omega R}\,; \qquad \text{II-46}$$

3) circuit losses should be such that

$$R < \frac{a_1 S}{\omega} \; ; \qquad \text{II-39}$$

4) the difference of non-linear capacitor potentials is given by

$$E_1 - E_2 = a_1 (1+S) \sqrt{\frac{S}{m}} \; ; \qquad \text{II-49}$$

5) the ratio of the two non-linear capacitor voltages is:

$$\frac{E_1}{E_2} = \Delta \left(1 + S - \frac{S}{\Delta^2} \right) ; \text{ and} \qquad \text{II-50}$$

6) the non-linearity should be such that

$$\frac{S}{S - m B^4} \geq \Delta > 1 \qquad \text{II-60}$$

does not require B so large that the component ratings are exceeded.

CHAPTER III

TWO-MESH, PARALLEL RESONANT CIRCUIT

The plan of this chapter is to develop relations for the two-mesh, parallel resonant circuit similar to those discussed in chapter II for the two-branch series resonant circuit. It will also be shown that the requirement of a constant-voltage source in the place of the previously used constant-current source gives rise to a different solution curve relating, A,B, and E_s, the source voltage.

As in chapter II, the first consideration will be the loss-free circuit and then the low-loss circuit.

SECTION 1: THE LOSS-FREE CIRCUIT

The equations for the circuit of figure I-1b can be written as follows:

$$i_o = \frac{\int e_1 dt}{L} + \frac{dq_1}{dt} \qquad \text{III-1a}$$

$$i_o = \frac{\int e_2 dt}{L} + \frac{dq_2}{dt}. \qquad \text{III-1b}$$

Subtracting equation III-1b from III-1a there is thus obtained one of the basic equations for the circuit:

$$\frac{1}{L}\int(e_1-e_2)dt + \frac{d(q_1-q_2)}{dt} = 0. \qquad \text{III-2a}$$

Since there are no d.c. sources in the circuit, no loss of generality occurs if equation III-2a is differentiated with respect to time. This differentiation results in

$$\frac{d^2(q_1-q_2)}{dt^2} + \frac{1}{L}(e_1-e_2) = 0. \qquad \text{III-2b}$$

This equation is the same as was obtained in chapter II for the two branch, series resonant circuit.

The other basic equation of the circuit is:

$$e_1 + e_2 = e_s . \qquad \text{III-3}$$

As with the series circuit, the defining relations for e_1 and e_2 are:

$$e_1 = a_1 q_1 + a_3 q_1^3, \qquad \text{III-4a}$$

$$e_2 = a_1 q_2 + a_3 q_2^3 \qquad \text{III-4b}$$

In lieu of the constant current source, a constant voltage source is desired. Hence C_1 should be fairly large. Thus, i_0 is a small quantity. For lossless circuits, e_1 and e_2 both lag i_0 by 90 degrees if $\omega > \omega_0$. The charge will be in phase with the voltage and the first approximations can be written as:

$$q_{10} = A\cos\omega t, \qquad \text{III-5a}$$

$$q_{20} = B\cos\omega t. \qquad \text{III-5b}$$

Proceeding as in chapter II, the two solution curves relating A and B are:

$$\psi_2 \equiv 0 = -S + m(A^2 + AB + B^2), \qquad \text{III-6}$$

$$\psi_4 \equiv 0 = -\frac{E_s}{a_1} + (A+B) + m(A^3 + B^3). \qquad \text{III-7}$$

It should be noted that the ψ_2 curve is common to both systems, but that the straight line, ψ_1, has now become the cubic ψ_4. These curves are shown in figure III-1, as derived in appendix II. The fact that ψ_4 is a cubic as shown, makes it possible to demonstrate bistability from the first iteration. The operating point for low values of E_s is on the intersection of ψ_4 and the line, A=B. As E_s is increased ψ_4 moves out from the β axis, its asymptotic line remaining parallel to the β axis. When ψ_4 becomes tangent to ψ_2 at P_1, the operating point "jumps" from P_1 to P_2 or P_3. Mathematical proof that P_1 is an unstable operating point is beyond the scope of this thesis. As stated in chapter II, however, the instability may be inferred from the work of Stoker [8]. The reasons leading to this conclusion of instability will now be shown.

In chapter II it was shown that the half axes of the ellipse are

$$a_\alpha = \sqrt{\frac{2S}{3m}}, \text{ and} \qquad \text{III-8}$$

$$a_\beta = \sqrt{\frac{2S}{m}}. \qquad \text{III-9}$$

The first of these represents the "distance" from the origin to P_1. Since A=B at this point:

$$A = \sqrt{\frac{S}{3m}}. \qquad \text{III-10}$$

Substituting this value into equation III-7 results in

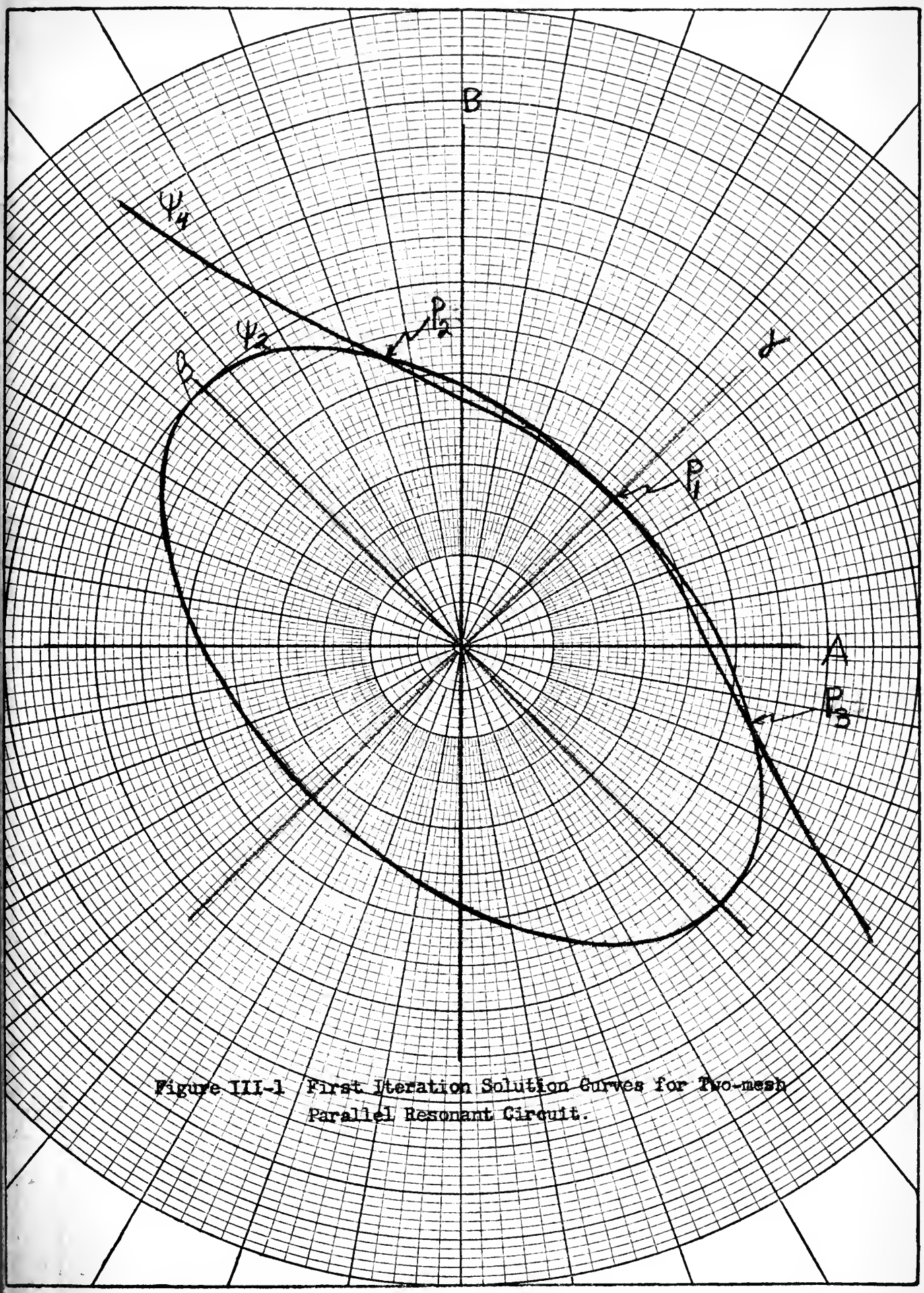

Figure III-1 First Iteration Solution Curves for Two-mesh Parallel Resonant Circuit.

$$E_s = 2a_1\left(1 + \frac{s}{3}\right)\sqrt{\frac{s}{3m}} \cdot \qquad \text{III-11}$$

As suggested in chapter II there is another method by which equation III-10 and hence equation III-11 may be derived. It is the criterion of this method which leads to the conclusion that, P_1 is unstable. In chapter I it was shown that the frequency for the loss-free Duffing equation was:

$$\omega^2 = a_1 + \frac{3}{4}a_3 A^2 - \frac{F}{A} \cdot \qquad \text{III-12}$$

Since Duffing's equation is the same as the equation for one mesh of the circuit under consideration if F is replaced by the voltage, E, across the mesh, the frequency is given by:

$$\omega^2 = \frac{a_1}{L} + \frac{3}{4}\frac{a_3}{L}A^2 - \frac{E}{A} \cdot \qquad \text{III-13}$$

The locus of the points where the curve of Fig. I-5b has vertical tangents can be obtained by differentiation of equation III-13 with respect to A and setting $d\omega/dA$ equal to zero. This procedure results in:

$$\omega^2 - \frac{a_1}{L} - \frac{9}{4}\frac{a_3}{L}A^2 = 0 \qquad \text{III-14}$$

The value of A, for a particular ω, which lies on the locus given by III-14 is found by solving equations III-13 and III-14 simultaneously. This results in the value of A,

$$A = \sqrt{\frac{s}{3m}} \cdot \qquad \text{III-10}$$

Stoker has shown that the region bounded by equation III-14 is unstable [8]. It was assumed that both meshes of the two-mesh circuit were identically designed, and that the circuit was supplied from

a constant voltage source. Thus, when A reaches the value given by III-10, only one of the mesh voltages can "jump" up. The other "jumps" down. Hence, P_1 is unstable and operation "jumps" to either P_2 or P_3.

The value of E_s given by equation III-11 has another interpretation which may be obtained by study of figure III-1. If E_s were larger than the value given by equation III-11, then there is the possibility of having two sets of bistable operating points, since Ψ_4 will intersect Ψ_2 in four points. Thus for no more than two possible stable operating points

$$E_s < 2a_1\left(1+\frac{S}{3}\right)\sqrt{\frac{S}{3m}} \cdot \qquad \text{III-15}$$

This apparent contradiction between equations III-15 and III-11 is explained as follows. Bistability results when E_s reaches the value given by equation III-11. However, as the amplitude of I_s is increased, there is no assurance that the value of E_s will increase due to the phase relationships possible between A and B. As stated in chapter II, operating points lying in the first quadrant represent the in phase conditions, whereas those operating points lying in the second or fourth quadrants represent the 180 degree phase conditions. However,if E_s can be caused to exceed the value given by equation III-12 after bistability has been reached, then four stable points may be possible.

As E_s is further increased, there is a value beyond which bistability will cease and reversion to the A=B condition occurs. This value of E_s is determined by finding the common point of tangency between Ψ_2 and Ψ_4 besides the one already found at P_1 . For Ψ_2 and Ψ_4 to osculate at a given point, the following relations must be satisfied at the point

$$\frac{\partial \psi_2}{\partial A} = \frac{\partial \psi_4}{\partial A}, \qquad \text{III-16}$$

$$\frac{\partial \psi_2}{\partial B} = \frac{\partial \psi_4}{\partial B} \qquad \text{III-17}$$

when Es has been adjusted so that the point of tangency lies on ψ_2, then both the necessary and sufficient conditions have been met.

Applying equations III-16 and III-17 to equations III-6 and III-7 there results, respectively:

$$1 + 3mA^2 = m(2A + B), \qquad \text{III-18}$$

$$1 + 3mB^2 = m(2B + A). \qquad \text{III-19}$$

Division of these two equations by each other, and simplification gives

$$3m(A^3 - B^3) + (6mAB - 1)(A - B) = 0. \qquad \text{III-20}$$

The solution A=B is trivial for the present development and hence there results:

$$\psi_5 \equiv 0 = A^2 + 3AB + B^2 - \frac{1}{3m} \qquad \text{III-21}$$

Application of the rotation matrix

$$\begin{bmatrix} A \\ B \end{bmatrix} = \begin{bmatrix} 1/\sqrt{2} & -1/\sqrt{2} \\ 1/\sqrt{2} & 1/\sqrt{2} \end{bmatrix} \begin{bmatrix} \alpha \\ \beta \end{bmatrix} \qquad \text{III-22}$$

to equation III-21 results in

$$\psi_5 \equiv 0 = 5\alpha^2 - \beta^2 - \frac{2}{3m} \qquad \text{III-23}$$

a hyperbola with half-axes.

$$b_\alpha = \sqrt{\frac{2}{15m}} \qquad \text{III-24}$$

$$b_\beta = \sqrt{\frac{2}{3m}}. \qquad \text{III-25}$$

The ellipse, ψ_2 and the hyperbola, ψ_5 will intersect if the half axes obey the relations

$$b_\alpha < a_\alpha \; ; \text{ or } \sqrt{\frac{2}{15m}} < \sqrt{\frac{25}{3m}} . \qquad \text{III-26}$$

From this inequality another criterion for bistability results:

$$S > \frac{1}{5}, \qquad \text{or} \qquad \text{III-27}$$

$$\omega^2 > \frac{6}{5}\omega_0^2. \qquad \text{III-28}$$

The two criteria for bistability, i.e. the required values of s and Es, thus far derived have been obtained from the first iteration.

The second iteration should give corrections to these relations. Proceeding as in chapter II the two solution curves thus obtained are:

$$\psi_3 \equiv 0 = -\frac{S}{m} + (A^2+AB+B^2) + D(A^4+A^3B+A^2B^2+AB^3+B^4) + 2D^2(A^6+A^5B+A^4B^2+A^3B^3+A^2B^4+AB^5+B^6) \qquad \text{III-29}$$

$$\psi_6 \equiv 0 = -\frac{Es}{a_1} + (A+B) + m(A^3+B^3) + mD(A^5+B^5) + 2mD^2(A^7+B^7). \qquad \text{III-30}$$

The curves are shown in figure III-2 Continuing the reasoning of the first iteration procedure, bistability occurs when ψ_6 becomes tangent to ψ_3 at P_1. Applying the rotation matrix, equation III-22 to equation III-29 and equation III-30 gives, respectively:

$$\psi_3 \equiv 0 = -\frac{S}{m} + \frac{1}{2}(3\alpha^2+\beta^2) + \frac{D}{4}(5\alpha^4+10\alpha^2\beta^2+\beta^4) + \frac{D^2}{4}(7\alpha^6+35\alpha^4\beta^2+21\alpha^2\beta^4+\beta^6), \qquad \text{III-31}$$

$$\psi_6 \equiv 0 = -\frac{E_1}{a_1} + \sqrt{2}\alpha + \frac{m}{\sqrt{2}}(\alpha^3+3\alpha\beta^2) + \frac{mD}{2\sqrt{2}}(\alpha^5+10\alpha^3\beta^2+5\alpha\beta^4) + \frac{mD^2}{2\sqrt{2}}(\alpha^7+21\alpha^5\beta^2+35\alpha^3\beta^4+7\alpha\beta^6). \qquad \text{III-32}$$

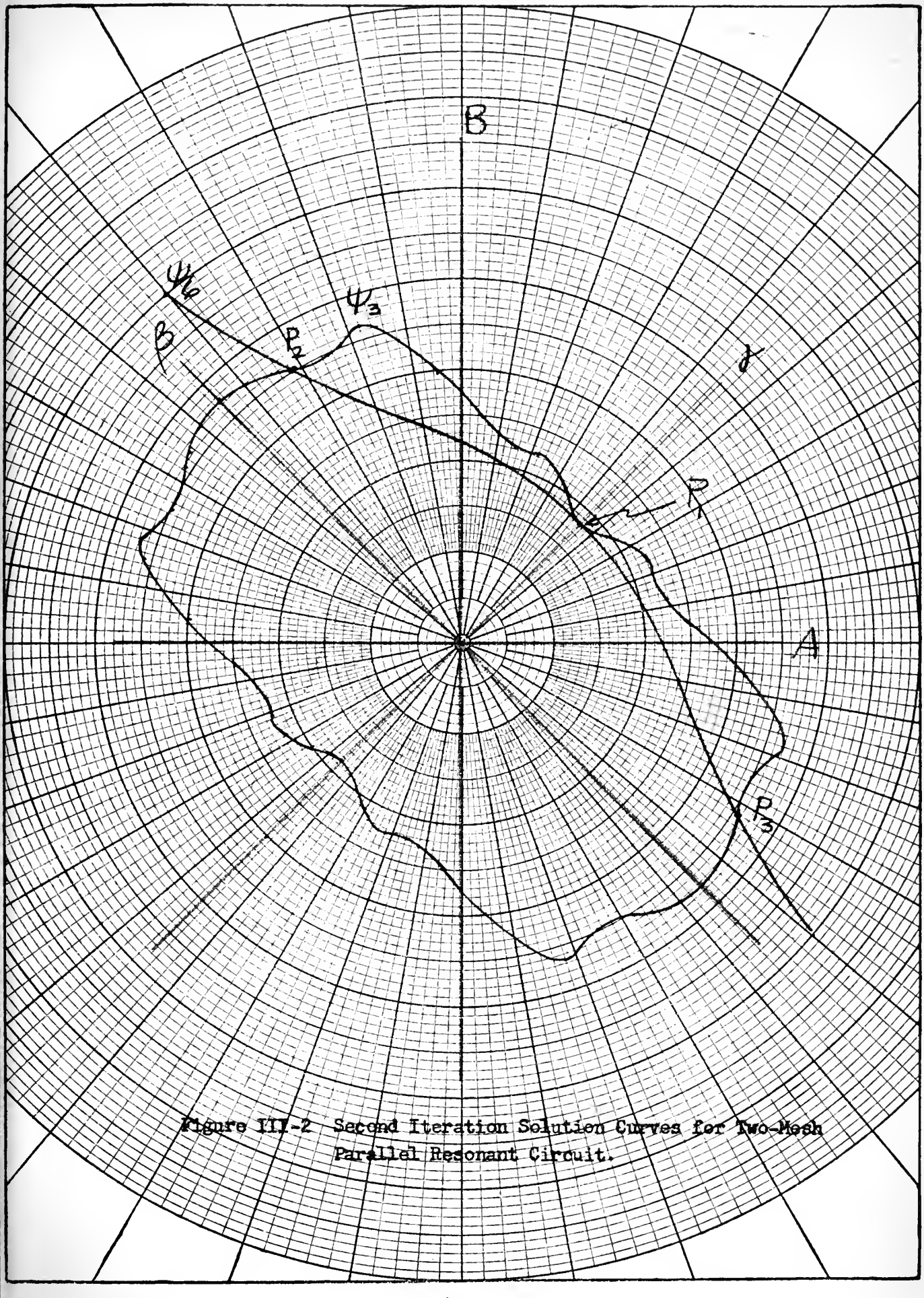

Figure III-2 Second Iteration Solution Curves for Two-Mesh Parallel Resonant Circuit.

As before, the solution curves are now brought into the polar form through the equations: $\alpha = \rho\cos\theta$ and $\beta = \rho\sin\theta$. This results in:

$$\Psi_3 \equiv 0 = -\frac{s}{m} + \frac{1}{3}f(\theta)\rho^2 + \frac{\Delta}{4}g(\theta)\rho^4 + \frac{\Delta^2}{4}h(\theta)\rho^6 \qquad \text{III-33}$$

$$\Psi_5 \equiv 0 = -\frac{\sqrt{2}E_s}{a_1} + 2\cos\theta\rho + m j(\theta)\rho^3 + \frac{m\Delta}{2}k(\theta)\rho^5 + \frac{m\Delta^2}{2}\ell(\theta)\rho^7 \qquad \text{III-34}$$

where, f(θ), g(θ), and h(θ) are as in chapter II; and

$$j(\theta) = 3\cos\theta - 2\cos^3\theta \qquad \text{III-35a}$$

$$k(\theta) = 5\cos\theta - 4\cos^5\theta \qquad \text{III-35b}$$

$$\ell(\theta) = 7\cos\theta + 14\cos^3\theta - 28\cos^5\theta + 8\cos^7\theta. \qquad \text{III-35c}$$

Figure III-2 shows a plot of these curves. The curve Ψ_6 differs but little from Ψ_5, except for large values of m or ρ. The curve Ψ_6 shown is therefore an approximation.

The value of E_S required for bistability is obtained by substituting into equation III-34 the values: $\theta = 0$ degrees and

$$\rho_{\theta=0^\circ} = \frac{.756}{\sqrt{D}}\left[1.68\sinh\mu - 0.417\right]^{1/2}, \qquad \text{III-36}$$

where $$\mu = \frac{1}{3}\sinh^{-1}\left(\frac{.9165 + .805}{s+1}\right). \qquad \text{III-37}$$

This procedure results in

$$E_S = \frac{a_1}{\sqrt{2}}\left(2\rho_1 + m\rho_1^3 + \frac{m\Delta}{2}\rho_1^5 + \frac{m\Delta^2}{2}\rho_1^7\right), \qquad \text{III-38}$$

where ρ_1 is given by equation III-36,

There is no easily derived correction for the required value of s. Application of equations III-16 and III-17 to equations III-29 and

III-30 results in an equation which is very tedious to solve. Considering the approximations first made regarding the Q-E relationship of the non-linear capacitor, the solution does not seem worthwhile.

SECTION 2: THE LOW-LOSS CIRCUIT

As in chapter II, attention is now given to the low-loss circuit as shown in figure III-3, with the phase relationships shown in figure III-4. Equation III-2b then is rewritten as:

$$(\ddot{q}_1-\ddot{q}_2)+\omega^2(q_1-q_2)=\omega^2(q_1-q_2)-\frac{1}{R}(\dot{e}_1-\dot{e}_2)-\frac{1}{L}(e_1-e_2) \qquad \text{III-39}$$

Assuming R to be large compared to Xc_1, the first iteration commences with the approximation:

$$q_{10}=A\cos\omega t \qquad \text{III-40a}$$

$$q_{20}=B\cos(\omega t+\delta) \qquad \text{III-40b}$$

Substituting these into the right hand side of equation III-39, and involving the conditions for periodicity there results:

$$\left[(\omega^2-\frac{a_1}{L})A-\frac{3a_3}{4L}A^3\right]\cos\omega t+\frac{\omega}{R}\left[a_1A+\frac{3}{4}a_3A^3\right]\sin\omega t$$
$$-\left[(\omega^2-\frac{a_1}{L})B-\frac{3a_3}{4L}B^3\right]\cos(\omega t+\delta)$$
$$-\frac{\omega}{R}\left[a_1B+\frac{3}{4}a_3B^3\right]\sin(\omega t+\delta)=0. \qquad \text{III-41}$$

Using the expansions of $\cos(\omega t+\delta)$ and $\sin(\omega t+\delta)$ and equating coefficients of like functions there results, since $\cos\delta\approx 1$:

$$\frac{\omega}{R}(a_1B+\frac{3}{4}a_3B^3)\sin\delta=(\omega^2-\frac{a_1}{L})(A-B)-\frac{3a_3}{4L}(A^3-B^3) \qquad \text{III-42a}$$

$$\left[(\omega^2-\frac{a_1}{L})B-\frac{3a_3}{4L}B^3\right]\sin\delta=-\frac{\omega}{R}\left[a_1(A-B)+\frac{3a_3}{4}(A^3-B^3)\right]. \qquad \text{III-42b}$$

Dividing equation III-42a by III-42b and subsequent simplification results in:

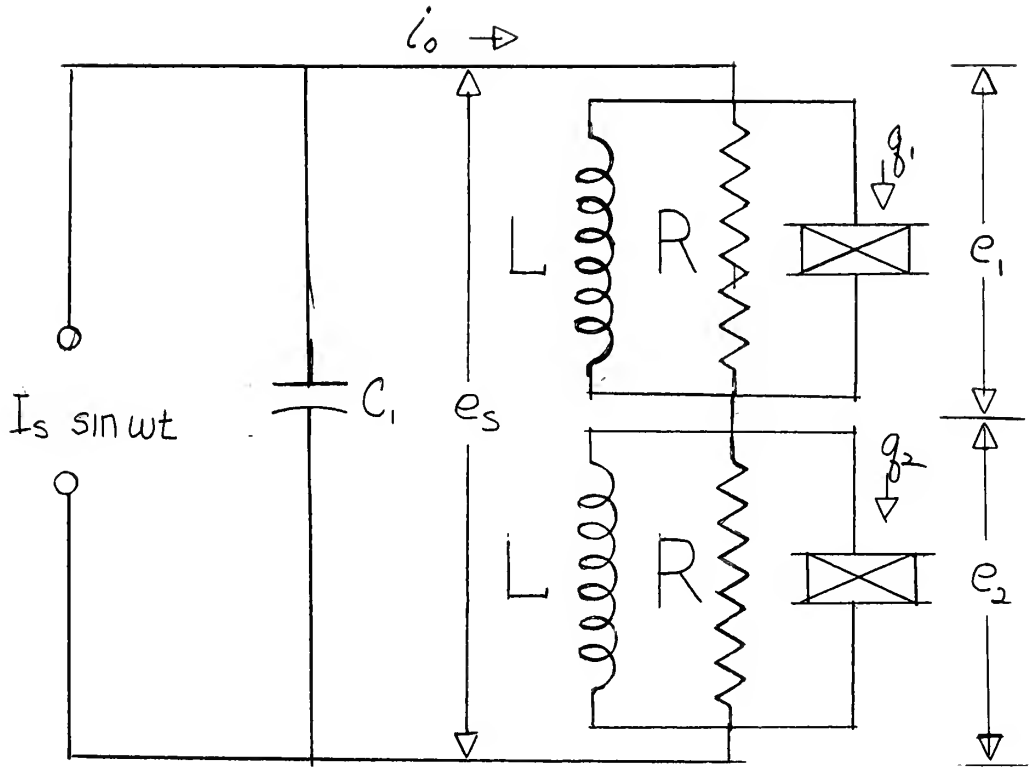

Figure III-3: Low-Loss, Two Mesh Parallel Resonant Circuit

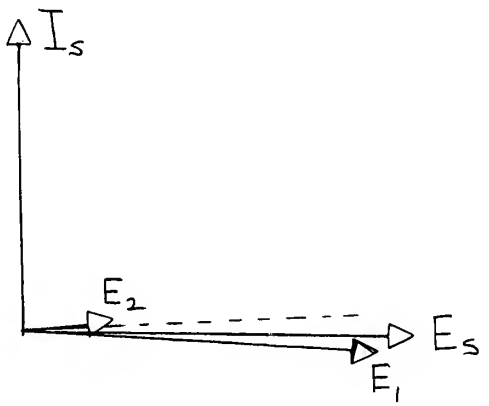

Figure III-4: Phase Relationship for Low-loss, Two-mesh Parallel Resonant Circuit.

$$-\frac{R^2}{\omega^2 L^2}\left(\frac{S+1}{1+mB^2}-1\right) = \frac{1+m(A^2+AB+B^2)}{S-m(A^2+AB+B^2)} \qquad \text{III-43}$$

Since in practice, mB^2 is of the order of 8×10^{-3} it can be neglected in comparison with unity. Thus equation III-43 reduces to

$$-\frac{R^2}{\omega^2 L^2} S = \frac{1+m(A^2+AB+B^2)}{S-m(A^2+AB+B^2)} . \qquad \text{III-44}$$

Solving this equation for A^2+AB+B^2 results in:

$$A^2+AB+B^2 = \frac{S^2+\frac{\omega^2 L^2}{R^2}}{m\left(S-\frac{\omega^2 L^2}{R^2}\right)} . \qquad \text{III-45}$$

Clearly this reduces to the loss-free case as R becomes infinite. If the right hand side of equation III-45 becomes negative, the equation fails to define a real ellipse. Thus in order to permit bistability, the following inequality must hold:

$$R > \frac{\omega L}{\sqrt{S}} . \qquad \text{III-46}$$

For $B \neq 0$, A is taken from III-45 as:

$$A = \sqrt{\frac{S^2+\frac{\omega^2 L^2}{R^2}}{m\left(S-\frac{\omega^2 L^2}{R^2}\right)}} . \qquad \text{III-47}$$

Solving equation III-1a for i_o, and using the fundamental component only results, after simplification, in the expression:

$$I_o = \frac{a_1}{R}\frac{\left(S^2+\frac{\omega^2 L^2}{R^2}\right)(S+1)}{\left(S-\frac{\omega^2 L^2}{R^2}\right)\sqrt{m\left(S-\frac{\omega^2 L^2}{R^2}\right)}} \qquad \text{III-48}$$

Since B is small, the admittance of the associated mesh is:

$$Y_2 = \frac{1}{\omega L}\sqrt{\frac{\omega^2 L^2}{R^2} + \left(\frac{\omega^2 L}{a_1} - 1\right)^2} = \frac{1}{\omega L}\sqrt{\frac{\omega^2 L^2}{R^2} + s^2}\,. \qquad \text{III-49}$$

Also, since B is small, there results from equation III-4b:

$$E_2 = a_1 B = \frac{I_0}{Y_2}\,, \quad \text{or} \qquad \text{III-50a}$$

$$B = \frac{\omega L}{R}\,\frac{(s+1)\sqrt{s^2 + \frac{\omega^2 L^2}{R^2}}}{\left(s - \frac{\omega^2 L^2}{R^2}\right)\sqrt{m\left(s - \frac{\omega^2 L^2}{R^2}\right)}} \qquad \text{III-50b}$$

Again, defining the switching ratio, Δ, as the ratio of A to B i.e. the ratio of the larger to the smaller charge amplitudes, there results:

$$\Delta = \frac{R}{\omega L}\,\frac{\left(s - \frac{\omega^2 L^2}{R^2}\right)}{s+1} \qquad \text{III-51}$$

Now, from equations III-4a and III-4b, and setting $B \approx 0$, there results:

$$E_1 = a_1 A + a_3 A^3 \qquad \text{III-52a}$$

$$E_2 = a_1 B. \qquad \text{III-52b}$$

Since the usefulness of this circuit is predicated upon a sufficiently large difference between the two mesh voltages, it may be desirable to solve for this voltage difference. Hence, by subtraction and use of equations III-47 and III-50b, there results:

$$E_1 - E_2 = \sqrt{\frac{s^2 + \frac{\omega^2 L^2}{R^2}}{m\left(s - \frac{\omega^2 L^2}{R^2}\right)}}\left\{a_1\left[1 - \frac{\omega L(s+1)}{R\left(s - \frac{\omega^2 L^2}{R^2}\right)}\right] + a_3\,\frac{s^2 + \frac{\omega^2 L^2}{R^2}}{m\left(s - \frac{\omega^2 L^2}{R^2}\right)}\right\}. \qquad \text{III-53}$$

For the loss-free case, this reduces to:

$$E_1 - E_2 = a_1\left(1 + \frac{4S}{3}\right)\sqrt{\frac{S}{m}} \quad . \qquad \text{III-54}$$

Here again, although the switching ratio is independent of the degree of non-linearity, m, the voltage difference is inversely proportional to its square root.

The ratio of the mesh voltages is given by

$$\frac{E_1}{E_2} = \Delta\left(1 + \frac{4}{3}\,\frac{S^2 + \frac{\omega^2 L^2}{R^2}}{S - \frac{\omega^2 L^2}{R^2}}\right). \qquad \text{III-55}$$

Since the second iteration of the low-loss circuit produces algebraic equations which are not readily solvable and the first, iteration of the low-loss circuit has become rather involved, it hardly seems reasonable to attempt a second iteration in an effort to obtain more information.

In summary, then, the following conclusions apply to the two-mesh parallel circuit:

1) The driving frequency must be such that for bistability to be possible,

$$\omega^2 > \omega_0^2; \qquad \text{III-28}$$

2) The minimum value of voltage required for bistability is, from the first iteration,

$$E_s = 2a_1\left(1 + \frac{S}{3}\right)\sqrt{\frac{S}{3m}}; \qquad \text{III-11}$$

3) The losses must be such that

$$R > \frac{\omega L}{\sqrt{S}}; \qquad \text{III-46}$$

4) The switching ratio is

$$\Delta = \frac{R}{\omega L}\,\frac{\left(s - \frac{\omega^2 L^2}{R^2}\right)}{s+1}\,; \qquad \text{III-51}$$

5) The voltage difference is given by

$$E_1 - E_2 = \sqrt{\frac{s^2 + \frac{\omega^2 L^2}{R^2}}{m\left(s - \frac{\omega^2 L^2}{R^2}\right)}}\left\{a_1\left[1 - \frac{\omega L(s+1)}{R\left(s - \frac{\omega^2 L^2}{R^2}\right)}\right] + a_3\,\frac{s^2 + \frac{\omega^2 L^2}{R^2}}{m\left(s - \frac{\omega^2 L^2}{R^2}\right)}\right\} \qquad \text{III-53}$$

6) The value of E_s required for bistability is, from the second iteration

$$E_s = \frac{a_1}{\sqrt{2}}\left(2\rho_1 + m\rho_1^3 + \frac{m}{2}\rho_1^5 + \frac{m}{2}D^2\rho_1^7\right) \qquad \text{III-38}$$

where

$$\rho_1 = \frac{.756}{\sqrt{D}}\left[1.68\sinh\mu - 0.417\right]^{1/2} \qquad \text{III-36}$$

and

$$\mu = \frac{1}{3}\sinh^{-1}\left(\frac{.9165 + .805}{s+1}\right) \qquad \text{III-37}$$

CHAPTER IV

USE OF TWO NON-LINEAR ELEMENTS: FIRST ITERATION

In chapters II and III, the two basic trigger-pair circuits utilizing a non-linear capacitor have been briefly studied. The two-mesh series resonant circuit, using a non-linear inductance, has been analyzed by Spitzer [7]. Intuitively it is felt that the inclusion of both types of non-linearities would reduce the currents required for the same switching ratio. This chapter will investigate this possibility by analyzing the loss-free, two-branch series resonant circuit using two non-linearities as shown in figure I-2. Due to the complexity of obtaining a solution and the inherent inaccuracies produced by the assumed current and charge functions, the analysis will be confined to the first iteration.

For reasons given in chapter I, the current-flux and charge-voltage relationships, are chosen as:

$$f(\phi) \equiv i = b_1 \phi + b_3 \phi^3 \qquad \text{IV-1}$$

$$g(q) \equiv e = a_1 q + a_3 q^3 \qquad \text{IV-2}$$

Furthermore, since

$$q = \int_0^t i \, dt, \qquad \text{IV-3}$$

equation IV-2 can be written as:

$$e = a_1\left[b_1\int_0^t \phi\,dt + b_3\int_0^t \phi^3\,dt\right] + a_3\left[b_1\int_0^t \phi\,dt + b_3\int_0^t \phi^3\,dt\right]^3. \qquad \text{IV-4}$$

One equation for the system is given by

$$N\frac{d(\phi_1-\phi_2)}{dt} + (e_1-e_2) = 0; \qquad \text{IV-5}$$

whereas the other equation is:

$$i_1 + i_2 = i_s \qquad \text{IV-6}$$

The branch currents and voltages are from equations IV-1 and IV-2 respectively:

$$i_1 = b_1\phi_1 + b_3\phi_1^3 \qquad \text{IV-7a}$$

$$i_2 = b_1\phi_2 + b_3\phi_2^3 \qquad \text{IV-7b}$$

$$e_1 = a_1 g_1 + a_3 g_1^3 \qquad \text{IV-8a}$$

$$e_2 = a_1 g_2 + a_3 g_2^3 \qquad \text{IV-8b}$$

Again, the capacitor, C_1, is to be the primary impedance offered to the driving voltage. Hence I_S leads E_S by 90 degrees. For the loss-free circuit, the branch currents will be in phase with the source current, I_S. Thus the branch fluxes will also be in phase with I_S, and the first approximation is taken as:

$$\phi_{10} = A\cos\omega t \qquad \text{IV-9a}$$

$$\phi_{20} = B\cos\omega t. \qquad \text{IV-9b}$$

Equation IV-5 can be differentiated with respect to time without affecting the solutions since there are no d.c. sources. After performing this differentiation, the equation is solved for $(\ddot{\phi}_1 - \ddot{\phi}_2)$.

In the resulting equation, $\omega^2(\phi_1-\phi_2)$ is added to both sides, and there is thus obtained:

$$(\ddot{\phi}_1-\ddot{\phi}_2)+\omega^2(\phi_1-\phi_2) = \omega^2(\phi_1-\phi_2)+\frac{1}{N}(\dot{e}_1-\dot{e}_2). \qquad \text{IV-10}$$

The iteration begins by substituting the approximations, ϕ_{10} and ϕ_{20} into the right hand side of equation IV-10 and then invoking the conditions for periodicity.

The most expedient way to do this is to write $\dot{e}$ as

$$\dot{e} = a_1 \frac{d(g)}{dt} + a_3 \frac{d(g^3)}{dt} . \qquad \text{IV-11}$$

The value of g is then obtained from equation IV-3 and the result cubed. The value of g^3 is then differentiated directly. This procedure eliminates the tedious progress of computing g^2 and then multiplying by $\dot{g}$.

From equation IV-3, using equations IV-9a and IV-9b there results:

$$g = \left[\frac{b_1}{\omega}(A-B) + \frac{3b_3}{4\omega}(A^3-B^3)\right]\sin\omega t + \frac{b_3}{12\omega}(A^3-B^3)\sin 3\omega t . \qquad \text{IV-12}$$

Letting

$$F = \frac{b_1}{\omega}\left[(A-B)+n(A^3-B^3)\right] \qquad \text{IV-13a}$$

and

$$G = \frac{b_1}{9\omega} n(A^3-B^3), \qquad \text{IV-13b}$$

there results upon cubing IV-12:

$$g^3 = \frac{3}{2}\left(\frac{F^3}{2}+FG^2\right)\sin\omega t - \frac{3}{4}(F^2G+G^2F)\cos 2\omega t$$

$$+ \frac{3}{2}\left(\frac{G^3}{2} + F^2G - \frac{F^3}{2}\right)\sin 3\omega t$$
$$+ \frac{3}{4}(F^2G + G^2F)\cos 4\omega t$$
$$- \frac{G^3}{4}\sin 9\omega t. \qquad \text{IV-14}$$

The condition for periodicity hence becomes

$$(A-B)\omega^2 + \frac{a_1 F}{N}\omega + \frac{3a_3}{2N}\omega\left(\frac{F^3}{2} + FG^2\right) = 0. \qquad \text{IV-15}$$

The terms F and G are replaced by equations IV-13a and IV-13b respecitvely and upon simplification there results:

$$-S/m(A-B) + \left(1 + \frac{lm}{m}\right)(A^3 - B^3) + 3lm(A^5 - B^5)$$
$$+ \frac{245}{81} lmn(A^7 - B^7) + \frac{83}{81} lmn^2(A^9 - B^9) = 0 \qquad \text{IV-16}$$

where

$$m = \frac{3}{4}\frac{a_3}{a_1} \qquad \text{IV-17a}$$
$$n = \frac{3}{4}\frac{b_3}{b_1} \qquad \text{IV-17b}$$
$$l = \frac{b_1^2}{\omega^2} \qquad \text{IV-17c}$$
$$S = \frac{\omega^2}{\omega_0^2} - 1 \qquad \text{IV-17d}$$
$$L_0 = N\left[\frac{d\phi}{dt}\right]_{\phi=0} = \frac{N}{b_1} \qquad \text{IV-17e}$$
$$C_0 = \left[\frac{dq}{dt}\right]_{q=0} = \frac{1}{a_1} \qquad \text{IV-17f}$$
$$\omega_0^2 = \frac{1}{L_0 C_0} = \frac{a_1 b_1}{N} \qquad \text{IV-17g}$$

The result of substituting equations IV-9a and IV-9b into IV-6 is:

$$I_s = b_1(A+B) + \frac{3b_3}{4}(A^3 + B^3). \qquad \text{IV-18}$$

This is the equation for ψ_4 found in chapter III. Omitting the trivial solution, A = B, equation IV-16 defines a solution curve, ψ_7. Bistability results when ψ_4 becomes tangent to ψ_7. This occurs at a point on the A = B line. To find the value of I_s required for bistability, equation IV-16 is first transformed into the polar coordinate form by the same transformations used in chapters II and III. The resulting equation is solved for $\rho_{\theta=0^\circ}$, and this value is used to compute A. Equation IV-18 then produces the required Is.

The transformations indicated above reduce equation IV-16 to

$$\psi_7 \equiv 0 = -\frac{s}{m} + \frac{1}{2}\left(1 + \frac{lm}{n}\right) f(\theta)\rho^2 + \frac{3}{4} lm\, g(\theta)\rho^4 + \frac{245}{324} lm\, n\, h(\theta)\rho^6 + \frac{83}{1296} lm\, n^2 p(\theta)\rho^8 \qquad \text{IV-19}$$

where $f(\theta), g(\theta)$ and $h(\theta)$ are defined as before, and

$$p(\theta) = 16\cos^8\theta - 64\cos^6\theta + 24\cos^4\theta + 32\cos^2\theta + 1. \qquad \text{IV-20}$$

If the term, ρ^8, is neglected, equation IV-19 is of the same form as the equation defining ψ_2. Since the functions involving the coordinate θ, are always positive, the effect of the second non-linearity is to reduce the required current for bistability. The amount of reduction depends on the value of l,m, and n.

There is no explicit statement derived, for the value which s must take. However, from previous developments of the single non-linearity circuit, it can be assumed that $s \overset{M}{>} 0$, at least.

Substituting the value θ = 0 degrees into equation IV-19 results in:

$$-\frac{s}{m} + \frac{3}{2}\left(1 + \frac{lm}{m}\right)\rho^2 + \frac{9}{2} lm\rho^4$$

$$+ \frac{1715}{324} lmn\rho^6 + \frac{83}{144} lmn^2\rho^8 = 0, \qquad \text{IV-20}$$

This equation is a quartic in ρ^2. The general form of the quartic is written as

$$x^4 + ax^3 + bx^2 + cx + d = 0, \qquad \text{IV-21}$$

where a,b,c and d are real, constant coefficients.

To find the roots of equation IV-21, it is necessary to find any real root of the cubic:

$$8y^3 - 4by^2 + 2(ac - 4d)y - [c^2 + d(a^2 - 4b)] = 0. \qquad \text{IV-22}$$

The roots of equation IV-21 are then taken from the two quadratics:

$$x^2 + \left[\frac{a}{2} - \sqrt{\frac{a^2}{4} + 2y_1 - b}\right]x + \left(y_1 + \sqrt{y_1^2 - d}\right) = 0 \qquad \text{IV-23a}$$

$$x^2 + \left[\frac{a}{2} + \sqrt{\frac{a^2}{4} + 2y_1 - b}\right]x + \left(y_1 - \sqrt{y_1^2 - d}\right) = 0 \qquad \text{IV-23b}$$

where y_1 is the root found in equation IV-22.

Obviously this is a tedious process. Fortunately, it needs to be done for only one value of θ. However, to arrive at a general solution in terms of the parameters l,m,n, and s is not within the realm of this thesis. For any given components and source frequency, the value of ρ obtained through the quadric solution is substituted into the polar form of equation IV-17:

$$\psi_4 \equiv 0 = -\frac{\sqrt{2}\, I_s}{b_1} + \frac{m}{2}(3\cos\theta - \cos 3\theta)\rho^3 + 2\cos\theta\,\rho. \qquad \text{IV-24}$$

This procedure gives the required value of I_s for bistability.

In summary, the results of analysis of the doubly non-linear series-resonant trigger pair are as follows:

1) The value of I_s should be less for bistability in the double non-linearity circuit than for the single non-linearity circuit;

2) There is no explicit development for the value which s should take, but it is implied by previous study that $s \gtrsim 0$.

3) The required value of I_s is obtained from auxiliary quartic, cubic and quadratic equations, as given by equations IV-20, IV-21 and IV-22.

CHAPTER V

EXPERIMENTAL RESULTS

The experimental results obtained with the circuits under consideration are given in this chapter. They are not offered especially to confirm theoretical developments, but to demonstrate that the circuits are operable. If the experiments agree with the theoretical developments, so much the better.

The charge-voltage relationships were determined through the use of the test equipment arrangement shown in figure V-1 for 60 cycle supply; and by the arrangement shown in figure V-2 for the 5 to 20 kilocycle range. Sample hysteresigrams for frequencies of 60, 5000, 10,000 and 20,000 cycles are shown in figure V-3. In figure V-4 is the hysteresigram taken at 60 cycles, but with the vertical gain and intensity set so that the loop characteristics are distinguishable. The locus of the tips of a nest of 20,000 cycle major hysteresis loops is shown in figure V-5.

For all experimental work the MUCON type VSE non-linear capacitors were used. The values of the coefficients for these type capacitors were obtained from figure V-5 by approximating the average initial and final slopes. The Q-E relationship resulting from this procedure is shown as the dashed curve in figure V-5.

The coefficient values thus obtained are

$$a_1 = 9 \times 10^8 \quad \text{volts/coul} \qquad \text{V-1a}$$

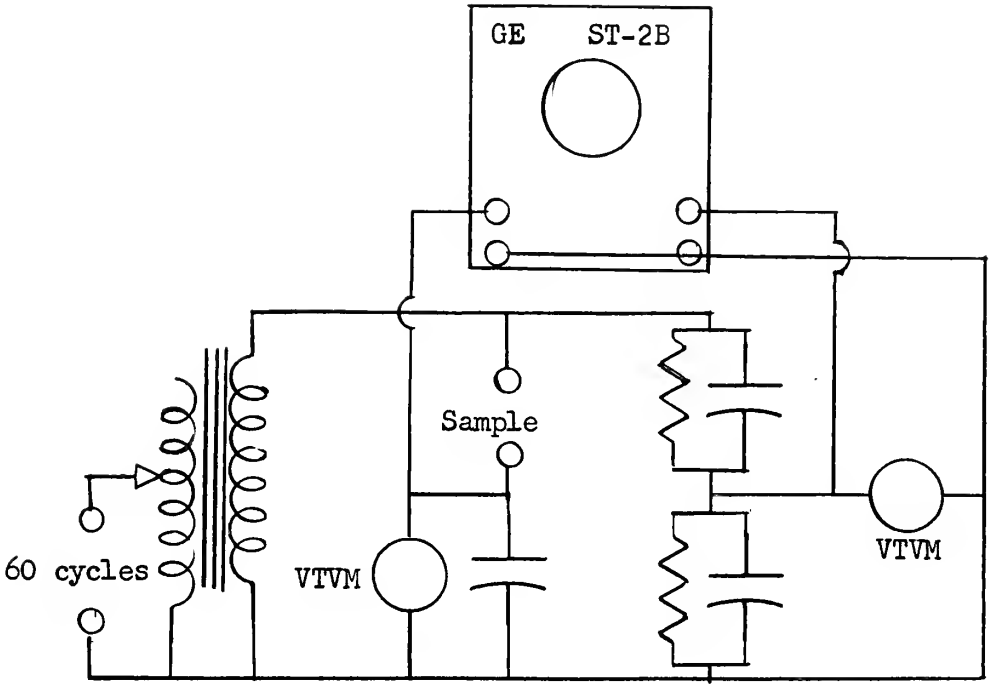

Figure V-1 Test Equipment for obtaining hysteresigram at 60 cycles. The VTVM should be peak reading.

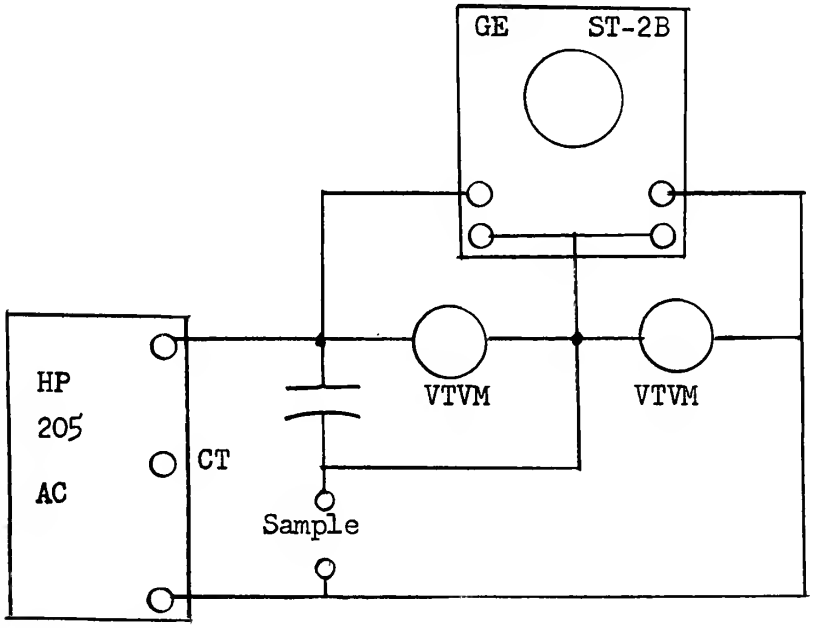

Figure V-2 Test equipment for obtaining hysteresigrams from 5 kcs to 20 kcs. The VTVM should be peak reading.

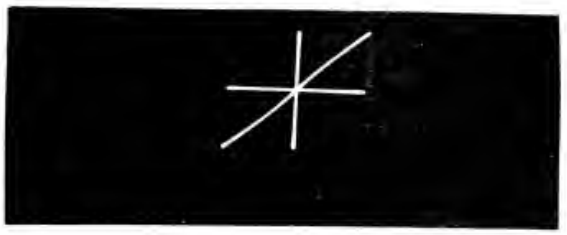

f: 20 kcs
Emax: 350 volts
Qmax: 0.27 ucoul.

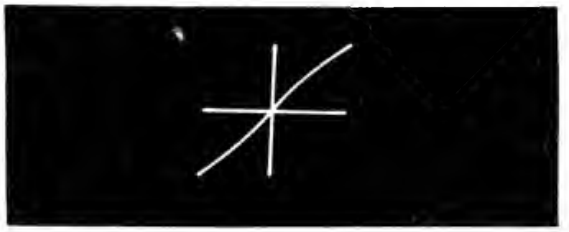

f: 10 kcs
Emax: 350 volts
Qmax: 0.3 ucoul.

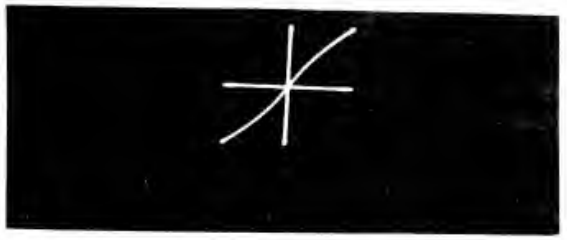

f: 5 kcs
Emax: 300 volts
Qmax: 0.299 ucoul.

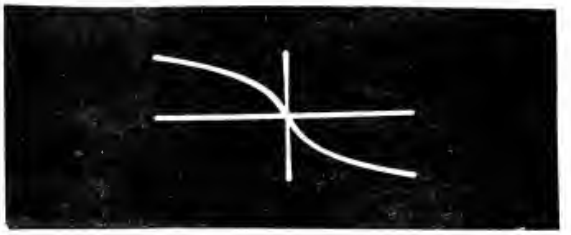

f: 60 cycles
Emax: 375 volts
Qmax: 0.315 ucoul.
(Q axis reversed)

Figure V-3. Hysteresigrams of MUCON type VSE non-linear capacitors.

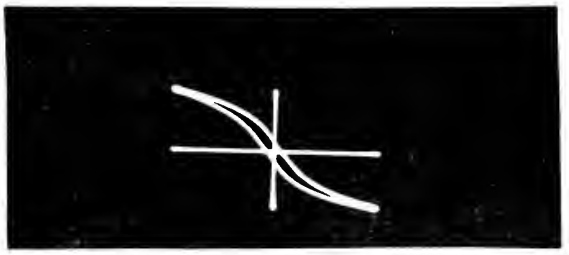

Figure V-4. Hysteresigram of MUCON type VSE non-linear capacitor showing open loop for a source frequency of 60 cycles.

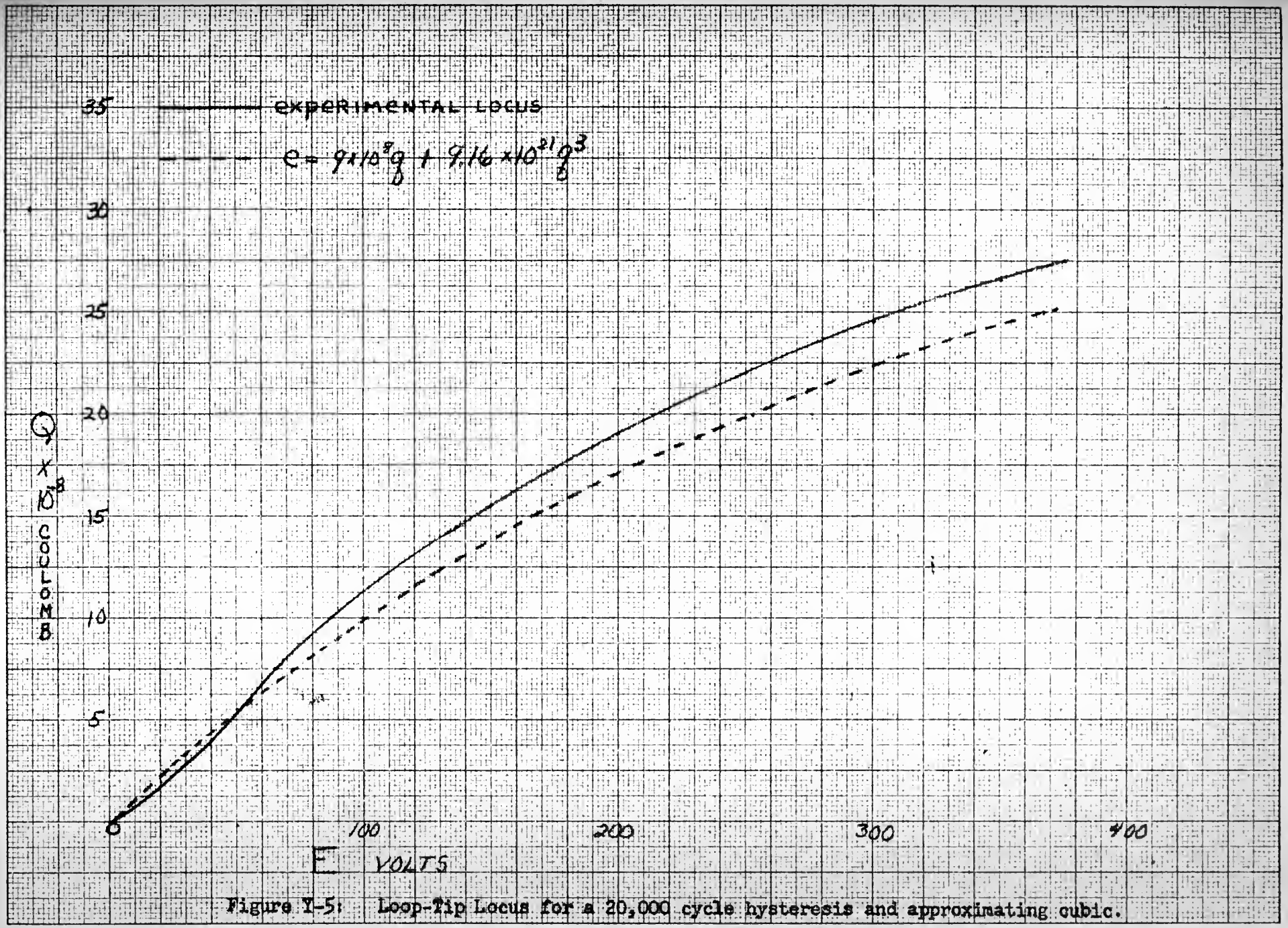

Figure I-5: Loop-Tip Locus for a 20,000 cycle hysteresis and approximating cubic.

$$a_3 = 9.16 \times 10^{21} \text{ volt}^{-1}/\text{coul}^3 \qquad \text{V-1b}$$

$$m = 7.63 \times 10^{12} \text{ coul}^{-2} \qquad \text{V-1c}$$

The circuit of figure I-1a was first tested using the following component values:

TEST NO.	1	2	3
L	110 mh	1.62 mh	0.46 mh
F	20 kcs	233 kcs	233 ks

For these components, the computed and experimental results are tabulated:

TEST	1	2	3
ω_i^2	8.18×10^9	5.55×10^{11}	1.96×10^{12}
S	0.94	2.86	.091
I_s (comp)	73 ma	1.59a	484 ma
I_s (exp)	70 ma	.544a	327 ma

Since the parameters, a_1 and a_3, were not separately determined for the higher frequency, it is not suprising that the experimental and theoretical results disagree. However, from tests two and three, it was noted that the higher value of s gave a quicker "jump" but that the temperature of the crystal oven in which the capacitors were located rose 10 degrees centigrade suggesting a radical change of the capacitor parameters as a function of temperature.

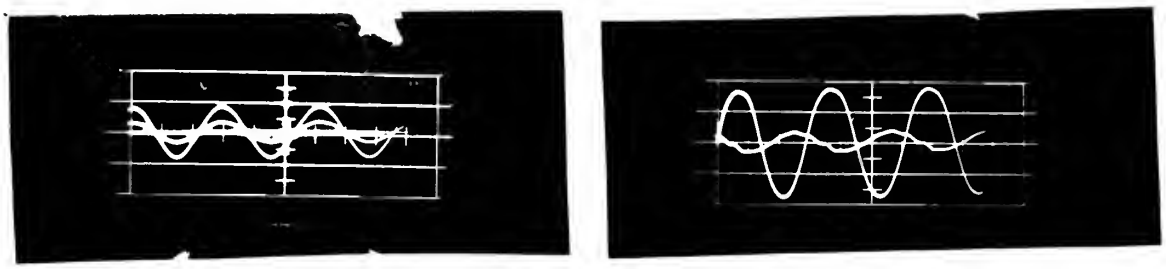

Figure V-6. E_1 and E_2 for the two-branch series resonant circuit. The source voltage is larger for the waveforms on the right.

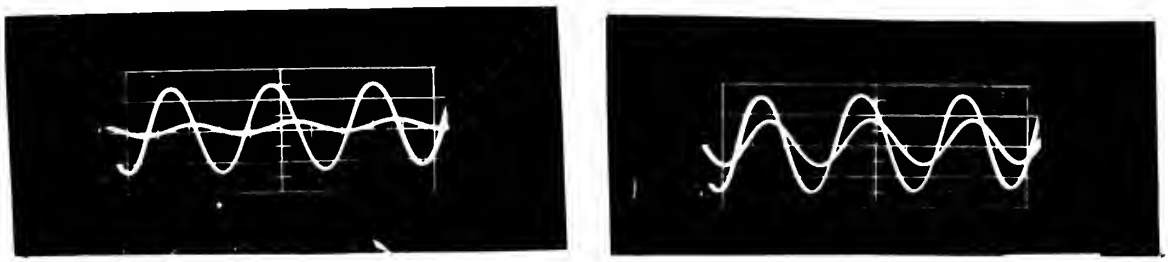

Figure V-7. E_1 and E_2 for the two-mesh parallel resonant circuit. The source current, I_s, is larger for the waveforms on the right.

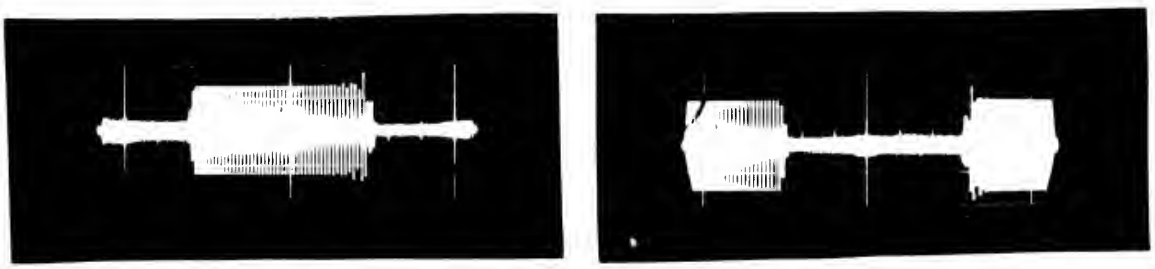

a b

Figure V-8. Relative switching ratios and switching rates of the single non-linear resonant circuit and the double non-linear circuit. Figure a shows the switch for the two-branch series resonant circuit using a non-linear inductance; figure b shows the switch for the two-branch series resonant circuit using both non-linear inductance and non-linear capacitance.

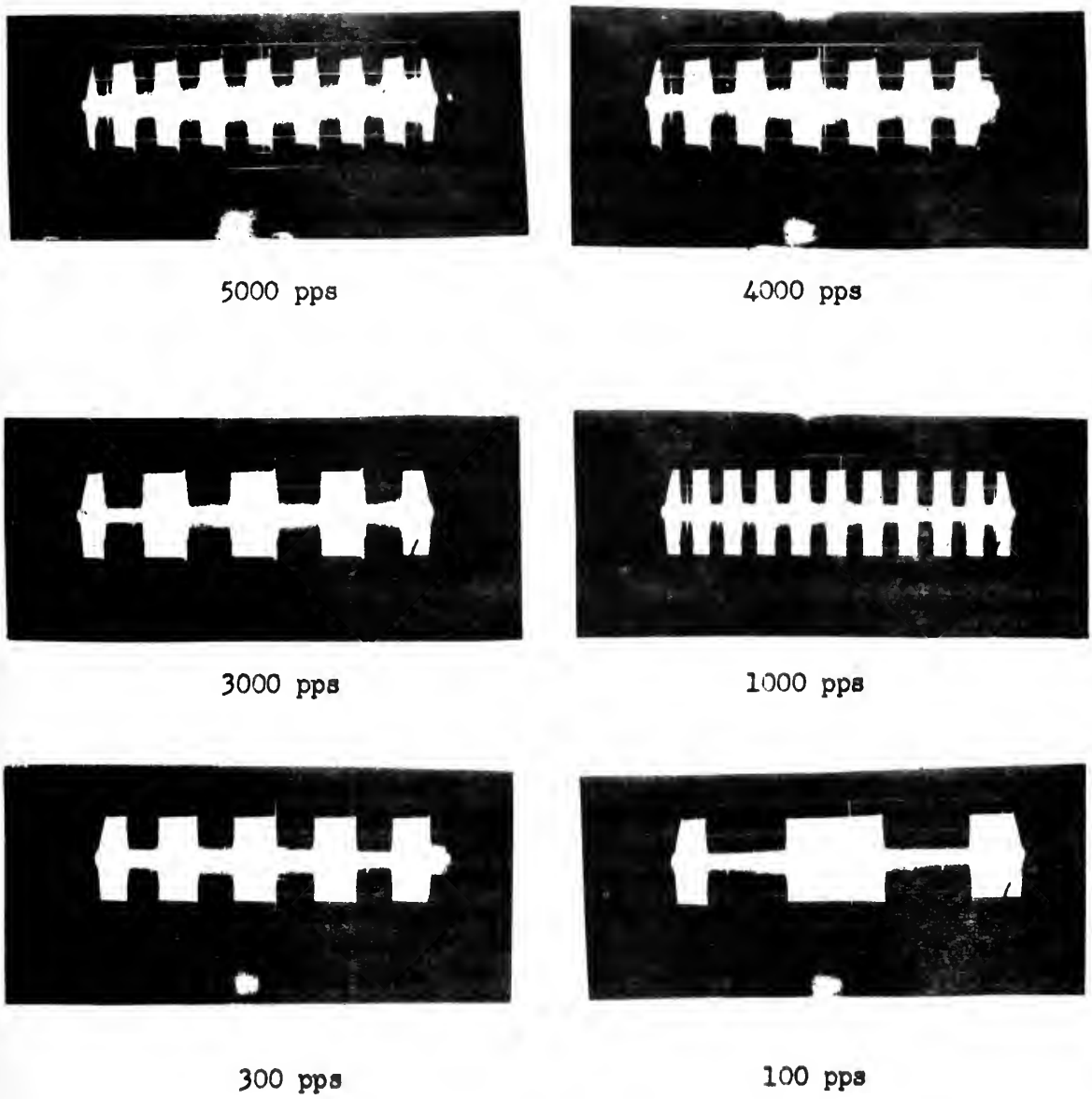

Figure V-9. Output voltage for various trigger rates of one branch of the two-branch series resonant circuit utilizing two non-linear elements. The voltage waveform is taken across one of the non-linear capacitors. The trigger pulse was 6.1 microseconds in duration and 65 volts in amplitude.

Switching was not obtainable by use of a pulse generator, but only by the use of a long-time (five seconds or more) short circuit across the high current capacitor. This indicates that the capacitors were heating excessively and that the subsequent change in parameter values was detrimental to switching. Methods of maintaining both capacitors at the same constant temperature were not feasible because of limitation of time available. Figure V-6 shows the output voltages E_1 and E_2 at 233 kcs after the bistability condition has been obtained. The phase relation conditions should be noted. The in-phase condition was first obtained, and by increasing Es, the out-of-phase condition resulted.

The parallel circuit was next investigated at the frequency of 20 kilocycles. The data on this test are given below.

TEST NO.	4
L	110 mh
ω_o^2	9.18×10^9
S	0.94
E_s (comp)	482 volts
E_s (exp)	578 volts

Figure V-7 shows the output voltages, E_1 and E_2 after the bistability condition has been obtained. Note that the two voltages begin out-of-phase and approach the in-phase condition as I_s is increased.

Losses in both the series resonant circuit and parallel resonant

circuit cause the large deviation from the 180 degree relationship.

The fifth test concerned itself with the double non-linear, two-branch series resonant circuit versus a single non-linear two-branch series resonant circuit. The non-linear inductors were those used by Spitzer [7]. The parameters of these were:

$$b_1 = 2 \times 10^4 \text{ amps/oer} \qquad \text{V-2a}$$

$$b_3 = 2 \times 10^{17} \text{ amps/oer}^3 \qquad \text{V-2b}$$

$$m = 7.5 \times 10^{12} \text{ oer}^{-2} \qquad \text{V-2c}$$

$$N = 200 \qquad \text{V-2d}$$

The capacitor replacing the non-linear capacitance for the single non-linearity circuit was chosen to give approximately the same switching ratio, .

The results are given below:

Test 5	Nonlinear Capacitor Linear Inductor	Nonlinear Capacitor Nonlinear Inductor
F	233 kcs	233 kcs
I_s	492 ma	475 ma

Figures V-8a and V-8b show the relative switching ratios and switching rates of the two circuits. The double non-linear circuit is shown to switch in about two cycles of the supply voltage whereas the circuit using only the non-linear inductance switches in about two and one-half cycles.

The sixth test consisted of operation of the double non-linear two-branch series resonant circuit at various switching rates. The results of this are shown in figure V-9. A Hewlitt-Packard Model 212A

Pulse generator was used as the trigger source.

Only during a brief interval of time was switching obtained on the two-branch series circuit using a non-linear capacitor. It was apparent from the experiments that the temperature change of the capacitors is the primary deterrent to switching.

It is felt that the data presented confirms the theory of the first four chapters to a good degree. The design equations seem to be valid for operation near the frequency region in which the capacitor parameters were determined. At high frequencies, the losses are so great in comparison to the degree of non-linearity, that the circuit does not operate within the theory propounded by the analysis.

BIBLIOGRAPHY

1. Gremer, C. E. — SOME ANALYTICAL METHODS OF SOLVING NON-LINEAR DIFFERENTIAL EQUATIONS, General Electric Technical Information Series No. R55ELP25 of 7 February 1955.

2. Kryloff, N. and Bogoliuboff, N. — INTRODUCTION TO NON-LINEAR MECHANICS, Princeton University Press, 1947 (a translation by S. Lefschetz).

3. Minorski, N. — NON-LINEAR MECHANICS, J. W. Edwards, Ann Arbor, 1947.

4. Pipes, L. A. — APPLIED MATHEMATICS FOR ENGINEERS AND PHYSICS, McGraw-Hill, New York 1947.

5. Pipes, L. A. — APPLICATIONS OF INTEGRAL EQUATIONS TO THE SOLUTION OF NON-LINEAR ELECTRIC CIRCUIT PROBLEMS, American Institute of Electrical Engineers, Transactions, Vol. 72 Part I 1953 pp. 445-450.

6. Pipes, L. A. — A MATHEMATICAL ANALYSIS OF A SERIES CIRCUIT CONTAINING A NON-LINEAR CAPACITOR, American Institute of Electrical Engineers, Transactions, Vol. 72 Part I, 1953 pp 238-242.

7. Spitzer, C. F. — THE FERRORESONANT TRIGGER PAIR: ANALYSIS AND DESIGN, General Electric Technical Information Series No. 54-E-292 of 27 October 1954.

8. Stoker, J. J. — NON-LINEAR VIBRATIONS, Interscience Publishers, Inc., New York 1950.

APPENDIX I

TRIGGERING SCHEMES

It was stated in chapters II and III that a circuit, in which controlled switching is obtainable between the two bistable points, would constitute a trigger pair. Obviously the circuit must also include means for obtaining this triggering. The purpose of this appendix is to present a few ideas as to how this may be obtained. The discussion will be limited to the suggested methods without too much thought as to their output requirements. One important question is left unanswered viz. by what method is memory produced. This is an important question, but is considered beyond the scope of this paper.

When the pendulum was studied in chapter I, it was found that the division between periodic and aperiodic solutions was dependent on the energy of the system. The circuits studied in chapters I, II, and III were shown to pass from the unistable condition to the bistable condition when a particular value of Es or Is was obtained. Although the implication was not forthright the approximation of the Q-E functions of these circuits to the sine function used in the pendulum case leads to the conclusion that the two states-unistable and bistable-are concerned with the amount of energy possessed by the individual branches or meshes.

As an approximation, only the energy contributed by the funda-

mental component will be considered.

Consider first, the two-branch series resonant circuit. There are two possible methods of trigger application: a pulse applied to the capacitor; or a pulse induced in the coil. In figure AI-1, both methods are shown.

From equation II-37, the value of A for which bistability occurs is given by

$$A = \frac{1}{\sqrt{3}} \sqrt{\frac{S}{m} - \frac{\omega^2 R^2}{a_1^2 S m}} \qquad \text{AI-1}$$

and from equation II-39 the value of A for the maximum Δ in the bistable condition is given by:

$$A_{max} = \sqrt{\frac{S}{m} - \frac{\omega^2 R^2}{a_1^2 S m}} \qquad \text{AI-2}$$

The current in one branch is ωQ_s and for each of the two states- unistable and bistable - it is given by:

$$I_1 = \omega A \qquad \text{AI-3a}$$

$$I_{1max} = \omega A_{max} \qquad \text{AI-3b}$$

Since the energy is associated with the magnetic field for part of the cycle of the driving frequency, the energy contained by the branch can be written:

$$U = \frac{1}{2} L I_1^2 = \frac{\omega^2}{2} L A^2 \qquad \text{AI-4a}$$

for the unistable state, or

$$U_{max} = \frac{\omega^2}{2} L A_{max}^2 \qquad \text{AI-4b}$$

for the bistable state.

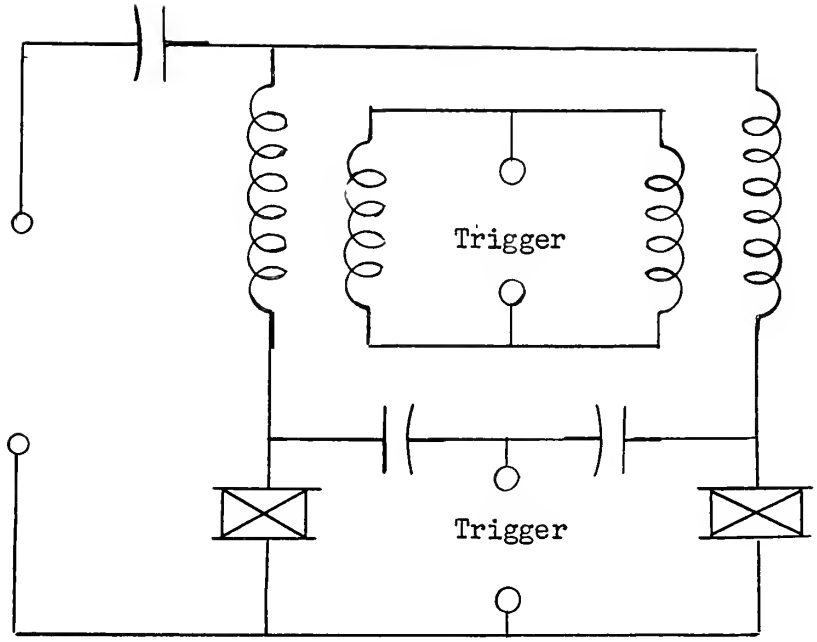

Figure AI-1 Two Trigger Schemes For Two Branch Series Resonant Circuit.

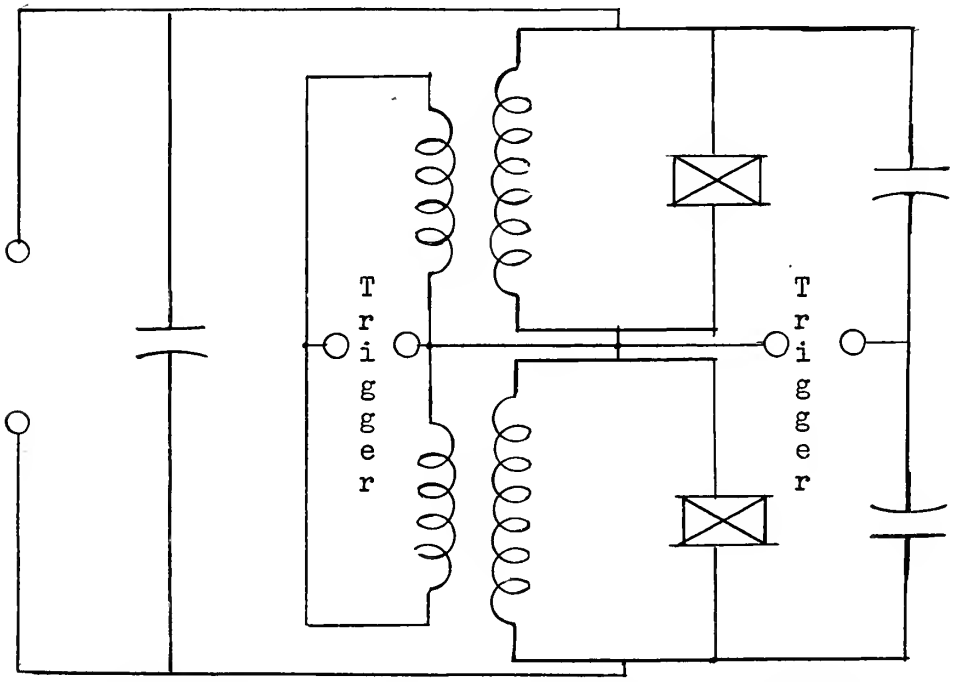

Figure AI-2 Two Trigger Schemes For Two-Mesh Parallel Resonant Circuit

The energy difference is thus given by:

$$U_{max} - U = \frac{\omega^2 L}{3m}\left(S - \frac{\omega^2 R^2}{a_1^2 S}\right) \qquad \text{AI-5a}$$

by using equations AI-1 and AI-2. This is the amount of energy that this branch must lose before it is possible to switch it into the lower charge state.

Since it was assumed that $B \neq 0$, the amount of energy this circuit must gain by virtue of a pulse is given from equation AI-4a as

$$\bar{U} = \frac{\omega^2 L}{6m}\left(S - \frac{\omega^2 R^2}{a_1^2 S}\right). \qquad \text{AI-6a}$$

When branch "1" has lost the amount of energy specified by equation AI-5a and branch "2" has simultaneously gained the amount specified by equation AI-6a, switching can occur. In order to assure switching, the equality should be replaced with the unequality sign as follows

$$U_{max} - U > \frac{\omega^2 L}{3m}\left(S - \frac{\omega^2 R^2}{a_1^2 S}\right) \qquad \text{AI-5b}$$

$$\bar{U} > \frac{\omega^2 L}{6m}\left(S - \frac{\omega^2 R^2}{a_1^2 S}\right). \qquad \text{AI-6b}$$

Since the trigger pulse is applied to both circuits, it must cause this exchange of energy to be as specified. At this point the investigation should inquire about memory. Although the subject memory is beyond the scope of this paper, a short attempt will be made to explain how the energy exchange may be caused.

The trigger pulse adds energy to both branches, "1" and "2". The addition of energy to branch "1" does not change the effective capaci-

tance of the non-linear element by much since it was already operating in the saturated region. However, the energy addition to branch "2" does cause a large change in the effecting capacitance of the non-linear element. Hence the opposition to the fundamental component decreases to the point of non-linear resonance in branch "2" but does not decrease appreciably in branch "1". Since the source is providing a constant current, the current now begins to divide between branches "1" and "2", adding to branch "2" by taking from branch "1". Branch "2" successively offers less opposition to the current whereas branch "1" successively increases its opposition. The process cascades until switching has occurred. When the energy in branch "1" has reached the value specified by equation AI-4a, the trigger pulse should cease. Otherwise it would be possible to have branch "1" return to its original state of heavy conduction. The reason for this is that the pulse is supplying a certain fixed amount of energy which must divide between the two branches. Since the effective capacity of the unsaturated branch is greater than that of the saturated branch, the unsaturated branch is more receptive to the energy. However, when the branches reach the energy level specified by equating AI-4a, the reception is equally well for both branches. Only the effect of cascading can then cause the switch.

The least amount of energy that the pulse must give is that specified by equation AI-6a. Since the energy will divide, and at some time, equally, perhaps the pulse energy required should be:

$$U_p = 2\bar{U} > \frac{\omega^2 L}{3m}\left(S - \frac{\omega^2 R^2}{a_1^2 S}\right). \qquad \text{AI-6c}$$

The required energy expression for the two-mesh parallel resonant circuit can be similarly obtained.

APPENDIX II

DERIVATION OF THE SECOND ITERATION SOLUTION CURVES

The purpose of this appendix is to show how the second iteration solution curves were obtained. The second iteration begins with the approximations:

$$g_{11} = A\sin\omega t - DA^3\sin 3\omega t \qquad \text{AII-1a}$$

$$g_{21} = B\sin\omega t - DB^3\sin 3\omega t. \qquad \text{AII-1b}$$

These are substituted into the right hand side of equation II-6, which after omission of the trivial solution, A=B, results in:

$$\Psi_3 \equiv 0 = -S + m(A^2+AB+B^2) + mD(A^4+A^3B+A^2B^2+AB^3+B^4)$$
$$+2mD^2(A^6+A^5B+A^4B^2+A^3B^3+A^2B^4+AB^5+B^6). \qquad \text{AII-2}$$

First, the linear transformation:

$$\begin{bmatrix} A \\ B \end{bmatrix} = \begin{bmatrix} 1/\sqrt{2} & -1/\sqrt{2} \\ 1/\sqrt{2} & 1/\sqrt{2} \end{bmatrix} \begin{bmatrix} \alpha \\ \beta \end{bmatrix} \qquad \text{AII-3}$$

is applied. This results in

$$\Psi_3 \equiv 0 = -\frac{S}{m} + \frac{1}{2}(3\alpha^2+\beta^2) + \frac{D}{4}(5\alpha^4+10\alpha^2\beta^2+\beta^4)$$
$$+ \frac{D^2}{4}(7\alpha^6+35\alpha^4\beta^2+21\alpha^2\beta^4+\beta^6). \qquad \text{AII-4}$$

This equation is next transformed into polar coordinate form by the relations $\alpha=\rho\cos\theta$ and $\beta=\rho\sin\theta$. This results in (see appendix III for expansion formulas):

$$\psi_3 \equiv 0 = -\frac{S}{m} + \frac{1}{2} f(\theta)\rho^2 + \frac{D}{4} g(\theta)\rho^4 + \frac{D^2}{4} h(\theta)\rho^6 \qquad \text{AII-5}$$

where

$$f(\theta) = 2 + \cos 2\theta \qquad \text{AII-6a}$$

$$g(\theta) = 3.5 + 2\cos 2\theta - 0.5\cos 4\theta \qquad \text{AII-6b}$$

$$h(\theta) = 15 + \cos 2\theta[4 - 18\cos 2\theta - \cos^2 2\theta] + 7\cos 4\theta. \qquad \text{AII-6c}$$

Equation AII-5 is now reduced to a cubic through the relation $\rho^2 = \Omega$. This results in:

$$\psi_3(\Omega) \equiv 0 = -\frac{S}{m} + \frac{1}{2} f(\theta)\Omega + \frac{D}{4} g(\theta)\Omega^2 + \frac{D^2}{4} h(\theta)\Omega^3. \qquad \text{AII-7}$$

From equations AII-6a, AII-6b, and AII-6c, it is noted that, for all θ, $f(\theta) > 0$, $g(\theta) > 0$ and $h(\theta) > 0$. Thus the terms of equation AII-7 varying in sign only as does Ω.

The coefficient signs are

$$\psi_3(\Omega): \quad - \quad + \quad + \quad +$$

$$\psi_3(-\Omega): \quad - \quad - \quad + \quad - \ .$$

Thus there is one or no possible positive roots; and there are two or no possible negative roots. Since there are three roots, it can be stated that there are two negative roots and one positive root. The interest lies entirely with the positive root since the negative roots produce complex values of ρ which have no meaning as far as the circuit is concerned. The "value" $\Omega = \infty$ does not satisfy the equation. Therefore ψ_3 is a single closed curve.

It now becomes necessary to find the real root of $\psi(\Omega)$.

The general form of a cubic equation is

$$a x^3 + 3b x^2 + 3c x + d = 0. \qquad \text{AII-8}$$

The trigonometric method of solving cubics is used and the real root is given by

$$x_1 = \frac{y_1 - b}{a}, \qquad \text{AII-9a}$$

where

$$\tfrac{1}{2} y_1 = \pm\sqrt{-g}\,\cos\left[\tfrac{1}{3}\cos^{-1}\frac{\pm h}{\sqrt{-g^3}}\right] \qquad \text{AII-9b}$$

if $g < 0$ and $g^3 + h^2 \le 0$;

$$\tfrac{1}{2} y_1 = \pm\sqrt{-g}\,\cosh\left[\tfrac{1}{3}\cosh^{-1}\frac{\pm h}{\sqrt{-g^3}}\right] \qquad \text{AII-9c}$$

if $g < 0$ and $g^3 + h^2 \ge 0$;

or

$$\tfrac{1}{2} y_1 = \pm\sqrt{g}\,\sinh\left[\tfrac{1}{3}\sinh^{-1}\frac{\pm h}{\sqrt{g^3}}\right] \qquad \text{AII-9d}$$

if $g > 0$;

and

$$g = ac - b^2; \qquad \text{AII-9e}$$

$$h = \tfrac{1}{2}(3acb - a^2 d) - b^3. \qquad \text{AII-9f}$$

The upper sign is chosen in the y_1 evaluation if $h > 0$ and the lower sign if $h < 0$. It turns out that for all θ, $g > 0$ and thus equation AII-9a is the vehicle by which the roots of ψ_3 are obtained.

The equations of $\psi_3(r)$ are tabulated below for values of θ.

θ	ψ_3 (r)			
0°	-s/m	$+ 1.5\, r$	$+1.25 D\, r^2$	$+1.75\, D^2 r^3$
10°	-s/m	$+ 1.47 r$	$+1.0\, D\, r^2$	$+1.86\, D^2 r^3$
20°	-s/m	$+1.385 r$	$+1.23 D\, r^2$	$+2.065 D^2 r^3$
30°	-s/m	$+1.25\, r$	$+1.19\, D r^2$	$+2.22\, D^2 r^3$

θ	$\Psi_3(r)$
40°	$-s/m + 1.09\,r + 1.07\,D\,r^2 + 2.15\,D^2r^3$
45°	$-s/m + r + 1.00\,D\,r^2 + 2\,D^2\,r^3$
50°	$-s/m + 0.913r + 0.905\,D\,r^2 + 2.07\,D^2r^3$
60°	$-s/m + 0.75\,r + 0.687\,D\,r^2 + 1.28D^2r^3$
70°	$-s/m + 0.617r + 0.470\,D\,r^2 + 0.753D^2r^3$
80°	$-s/m + 0.53\,r + 0.31D\,r^2 + 0.37\,D^2r^3$
90°	$-s/m + 0.5\,r + 0.25D\,r^2 + 0.25\,D^2r^3$

From these equations, the value of ρ is obtained for each angle specified

θ	ρ	$(u=\frac{1}{3}\sinh^{-1}\omega)$	ω
θ	$\pm \frac{.756}{\sqrt{D}}\left[1.68\sinh u - .417\right]^{1/2}$		$\frac{.916\,S + .805}{S+1}$
10°	$\pm \frac{.734}{\sqrt{D}}\left[1.79\sinh u - .333\right]^{1/2}$		$\frac{.683\,S + .583}{S+1}$
20°	$\pm \frac{.695}{\sqrt{D}}\left[1.788\sinh u - .41\right]^{1/2}$		$\frac{.955\,S + .825}{S+1}$
30°	$\pm \frac{.67}{\sqrt{D}}\left[1.75\sinh u - .397\right]^{1/2}$		$\frac{.871\,S + .72}{S+1}$

θ	ρ	$(\mu = \frac{1}{3}\sinh^{-1}\omega)$	ω
40°	$\pm \frac{.683}{\sqrt{D}}\left[1.51\sinh\mu - .356\right]^{1/2}$		$\frac{1.1S+.875}{S+1}$
45°	$\pm \frac{.707}{\sqrt{D}}\left[1.49\sinh\mu - .333\right]^{1/2}$		$\frac{.882S+.687}{S+1}$
50°	$\pm \frac{.695}{\sqrt{D}}\left[1.47\sinh\mu - .302\right]^{1/2}$		$\frac{.648S+.874}{S+1}$
60°	$\pm \frac{.885}{\sqrt{D}}\left[1.13\sinh\mu - .229\right]^{1/2}$		$\frac{.884S+.637}{S+1}$
70°	$\pm \frac{1.15}{\sqrt{D}}\left[.724\sinh\mu - .156\right]^{1/2}$		$\frac{7.89S+7.63}{S+1}$
80°	$\pm \frac{1.64}{\sqrt{D}}\left[.468\sinh\mu - .103\right]^{1/2}$		$\frac{.917S+.697}{S+1}$
90°	$\pm \frac{2}{\sqrt{D}}\left[.424\sinh\mu - .0833\right]^{1/2}$		$\frac{6.15S+4.82}{S+1}$

These are the only values needed to form a plot, since ψ_3 is symmetrical about both the α axis and β axis as can be seen from equation AII-4.

The plots in figures II-1 and III-2 were obtained from the above tabulations for an s value of 0.68. Although not labeled, the coordinates are in units of $m^{-\frac{1}{2}}$.

The development of ψ_4 and ψ_6 is done in a similar fashion. Tabulated equations of ψ_4, for values of θ are given below. Since ψ_6 differs from ψ_4 but little, except for large values of ρ or m, it has not been tabulated. The only real interest lies in the fact that both ψ_4 and ψ_6 have only one real positive root. For the value θ = 90 degrees, all coefficients of ρ vanish. Hence, ψ_4 and ψ_6 are open curves. Since they were derived from monotonically decreasing functions, $e_1(q)$ and $e_2(q)$ by a linear substitution, they will also be monotonically decreasing functions about the axis of symmetry. Hence the shape is as shown in figures III-1 and III-2.

θ	ψ_4
0°	$\frac{-\sqrt{2}\,E_s}{a_1} + 2\rho + m\rho^3$
10°	$-\frac{\sqrt{2}\,E_s}{a_1} + 1.97\rho + 1.05\,m\rho^3$
20°	$-\frac{\sqrt{2}\,E_s}{a_1} + 1.88\rho + 1.16\,m\rho^3$

θ	ψ_4
30°	$-\frac{\sqrt{2}E_s}{a_1} + 1.73\rho + 1.3m\rho^3$
40°	$-\frac{\sqrt{2}E_{s1}}{a_1} + 1.53\rho + 1.4m\rho^3$
45°	$-\frac{\sqrt{2}E_s}{a_1} + 1.41\rho + 1.41m\rho^3$
50°	$-\frac{\sqrt{2}E_s}{a_1} + 1.27\rho + 1.4m\rho^3$
60°	$-\frac{\sqrt{2}E_s}{a_1} + \rho + 1.75m\rho^3$
70°	$-\frac{\sqrt{2}E_s}{a_1} + 0.684\rho + 0.08m\rho^3$
80°	$-\frac{\sqrt{2}E_s}{a_1} + 0.348\rho + 0.01m\rho^3$
90°	$-\frac{\sqrt{2}E_s}{a_1} + 0\rho + 0m\rho^3$

Using the method previously described for finding roots of the cubic, there arise solutions such as

$$x_1 = \frac{b}{\sqrt{m}} \sinh\left[\frac{1}{3}\sinh^{-1} c\sqrt{m}\frac{E_s}{a_1}\right], \qquad \text{AII-10}$$

where b and c are constants determined for each value of θ. For values of $\frac{c\sqrt{m}E_s}{a_1} << 1$, the approximation

$$\sinh^{-1}x = \ln(x+\sqrt{x^2+1}) \approx \ln(x+1) \qquad \text{AII-11}$$

can be used. Since the approximation specifies $x^2 < 1$, there is the series equality:

$$\ln(x+1) = x - \tfrac{1}{2}x^2 + \tfrac{1}{3}x^3 - \tfrac{1}{4}x^4 + \cdots \qquad \text{AII-12}$$

Using only the first term of AII-12, equation AII-10 becomes

$$x_1 \approx \frac{b}{\sqrt{m}} \sinh \frac{c}{3}\frac{\sqrt{m}E_s}{a_1}. \qquad \text{AII-13}$$

Again since $\frac{c\sqrt{m}E_s}{a_1} << 1$, the hyperbolic sine function can be replaced by the first term of its power series expansion. Thus

$$x_1 \approx \frac{b c E_s}{3a_1} \qquad \text{AII-14}$$

For the values of m and a_1 used in experiments, Es should be less than 100 volts for all the approximations to be valid. It was on this basis that ψ_4 and ψ_6 were plotted in figures III-1 and III-2 respectively. It is not anticipated that a marked difference would result if the value of Es were such that equation AII-10 must be used.

The slope of the ψ_3 curve is obtained by application of the formula

$$\tan T = \frac{\rho' \sin\theta + \rho\cos\theta}{\rho'\cos\theta + \rho\sin\theta}, \qquad \text{AII-15}$$

where T is the angle the tangent makes with the horizontal axis. Since the horizontal axis is the α axis, for the tangent to be parallel to the β axis, the denominator of AII-15 must vanish, or the numerator must become infinite.

Differentiating AII-5 with respect to θ, there results:

$$\psi_3' \equiv 0 = \left[f(\theta) + D g(\theta) \rho^3 + \frac{3}{5} D^2 h(\theta) \rho^5 \right] \rho' - \left[\frac{f'(\theta)}{2} \rho^2 + \frac{D}{4} g'(\theta) \rho^4 + \frac{D^2}{4} h'(\theta) \rho^6 \right]. \qquad \text{AII-16}$$

From equations AII-6a, AII-6b and AII-6c, it can be seen that $f'(\theta)$, $g'(\theta)$ and $h'(\theta)$ each have the factor sin θ, sin 2θ, or sin 4θ. Thus, ρ' vanishes for $\theta = 0$ degrees and therefore so does the denominator of AII-15. It has then been proven that the tangent of ψ_3 at P_1 is parallel to the axis.

APPENDIX III

MATHEMATICAL FORMULAS USED IN ANALYSIS

This appendix lists, for the readers' reference, mathematical formulas used in the analytical portion of this paper.

The trigonometric expansions are obtained by applying the binominal expansion to the exponential form of the sine and cosine functions. Thus there results

$$(\sin nx)^{2m} = \left[\frac{\epsilon^{jnx} - \epsilon^{-jnx}}{2j}\right]^{2m} \qquad \text{AIII-1a}$$

$$(\sin nx)^{2m} = \frac{(-1)^m}{2^{2m}} C_m^{2m} + \frac{1}{2^{2m-1}}\Big\{\cos 2mnx - C_1^{2m}\cos 2(m-1)nx + \cdots\cdots + (-1)^r C_r^{2m}\cos 2(m-r)nx + \cdots\Big\} \qquad \text{AIII-1b}$$

$$(\cos nx)^{2m} = \left[\frac{\epsilon^{jnx} + \epsilon^{-jnx}}{2}\right]^{2m} \qquad \text{AIII-2a}$$

$$(\cos nx)^{2m} = \frac{1}{2^{2m}} C_m^{2m} + \frac{1}{2^{2m-1}}\Big\{\cos 2mnx + C_1^{2m}\cos 2(m-1)nx + \cdots\cdots + C_r^{2m}\cos 2(m-r)nx + \cdots\Big\} \qquad \text{AIII-2b}$$

$$(\sin n\chi)^{2m+1} = -\frac{1}{2^{2m}}\left\{\sin(2m+1)n\chi - C_1^{2m+1}\sin(2m-1)n\chi + \cdots\cdots + (-1)^n C_n^{2m+1}\sin(2m+1-2n)n\chi + \cdots\right\} \quad \text{AIII-3}$$

$$(\cos n\chi)^{2m+1} = \frac{1}{2^{2m}}\left\{\cos(2m+1)n\chi + C_1^{2m+1}\cos(2m-1)n\chi + \cdots\cdots + C_n^{2m+1}\cos(2m+1-2n)n\chi + \cdots\right\} \quad \text{AIII-4}$$

In determining that ψ_2 was an ellipse and investigating if it became an imaginary ellipse due to the presence of losses, the following properties of conic sections were used.

The general form of a conic is written as

$$ax^2 + 2hxy + by^2 + 2gx + 2fy + c = 0. \quad \text{AIII-5}$$

The relations, D, d and c are defined as:

$$D = \begin{vmatrix} a & h & g \\ h & b & f \\ g & f & c \end{vmatrix} \quad \text{AIII-6a}$$

$$d = \begin{vmatrix} a & h \\ h & b \end{vmatrix} \quad \text{AIII-6b}$$

$$e = a + b \qquad \text{AIII-6c}$$

The conic is:

1. a parabola if $d = 0$, $D \neq 0$;
2. parallel lines (may be coincident or imaginary) if $d = 0$, $D = 0$;
3. an ellipse if $d > 0$, $eD < 0$;
4. no locus (imaginary ellipse) if $d > 0$, $eD > 0$;
5. a point ellipse if $d > 0$, $D = 0$;
6. an hyperbola if $d < 0$, $D \neq 0$
7. two intersecting lines if $d < 0$, $D = 0$.

In order to remove the xy term of the generalized conic equation, the rotation matrix

$$\begin{bmatrix} A \\ B \end{bmatrix} = \begin{bmatrix} \cos\theta & -\sin\theta \\ \sin\theta & \cos\theta \end{bmatrix} \begin{bmatrix} \alpha \\ \beta \end{bmatrix} \qquad \text{AIII-7}$$

is applied, where θ is given by

$$\tan 2\theta = \frac{2h}{a-b} \qquad \text{AIII-8}$$